The Hebrew University of Jerusalem,

the Faculty of Mathematics and

Sciences

Department of Applied Physics

Simulation and analysis of a soliton perturbation by a truncated Airy in Kerr media

חקר וניתוח של הפרעה של סוליטון על ידי איירי קטום בתווך לא ליניארי

Thesis by:Amitay Rudnick

Advisor: D"r Dan Marom

Abstract

The simulation and analysis of a temporal soliton perturbation (interaction) with a dispersive truncated Airy pulse traveling in a nonlinear fiber at the same center wavelength (or frequency). True Airy pulses remain self-similar while propagating along a ballistic trajectory. However, they are infinite in energy due to the infinite tail that prevents the energy integral from converging. In order to be realized, Airy pulses must therefore, be truncated. The truncation is carried out by apodizing the infinite Airy tail. Despite the truncation Airy pulses remain self-similar over extended ranges while the ballistic trajectory is completely preserved. This allows them to interact with a nearby soliton on account of the accelerating wavefront property.

The interactions are governed by the Nonlinear Schrödinger equation for which no analytical solution currently exists for these initial conditions. Therefore, numerical simulations are required. The numerical method chosen is the split step Fourier method which is a mathematical algorithm for propagation of the pulses. By providing the simulation program with the initial launch conditions we are able to follow the interactions as they progress.

Analysis of the simulation is carried out by tracking the fundamental parameters of the emergent soliton during propagation—time position, amplitude, phase and frequency—that alter due to the primary collision with the Airy main lobe and the continuous co-propagation with the dispersed Airy background. Following the collision, the soliton intensity oscillates as it relaxes in the dispersed Airy background, trying to settle in to a new soliton state. Further, by varying the initial parameters of the Airy pulse such as initial phase, amplitude and time position, different outcomes are witnessed which allows for a broader understanding of the interaction.

Due to the spectral repositioning of the Airy spectrum by dispersion, the interaction is found to resemble coherent interactions at times and incoherent at others. The results indicate that in certain cases permanent change in frequency and intensity occurs, depending on the configuration of the initial parameters chosen. These changes are made apparent through changes in time position and in the accumulated phase of the soliton. Furthermore, according to the perturbation theory local changes in time position and phase can also occur independently from the frequency change and intensity change, respectively.

תקציר

מחקר זה עוסק בהתנגשויות ואינטראקציה בין שני פולסים; פולס סוליטון ואיירי נפיץ וקטום. פולסים אלו הינם בעלי אותו תדר נושא והם מתקדמים בתוך סיב אופטי לא ליניארי. פולס איירי הינו בעל שני תכונות יוצאות דופן; הוא משמר את צורתו במהלך התקדמותו ומתקדם לאורך מסלול בליסטי, אך אינו בר קיימא כיוון שנדרשת אינסוף אנרגיה על מנת לשמרו . כדי להפכו לממשי נדרשת קטימה של הזנב האין סופי המתבצע על ידי הכפלת הזנב באקספוננט דועך. עם זאת, למרות הקטימה נמצא שהתכונה של שימור צורתו במהלך התקדמותו נשמרת לאורך מרחק רב ויכולת האצה אינה נפגעת כלל. על כן, פולס אייר מסוגל להאיץ, להתנגש בפולס סוליטון המקורב לו ולאחר מכן לעבור עמו אינטראקציה.

אופי האינטראקציה מוכתב על ידי מה שמכונה המשוואה הלא ליניארית של שרדינגר ולעת עתה לא קים פתרון אנליטי לתאי התחלה אלו. כדי לדמות את מהלך אינטראקציות אלו אני נעזר בשיטת המכונה ספליט-סטפ פורייה (split-step Fourier method). שיטה זו הינה אלגוריתם מתמטי לקידום הפולסים בעזרת התמרת פורייה. בהינתן תנאי התחלה לתוכנית הקידום ניתן לעקוב אחרי התפתחות האינטראקציה והתנהגותה.

ניתוח הסימולציה נעשה בעזרת מעקב אחר התכונות הבסיסיות של פולס הסוליטון במהלך ההתנגשות ולאחריה. התכנות הבסיסיות של סוליטון הינן; המיקום הזמני שלו (המומנט הזמני הראשון), עוצמה, פאזה והתדר הנושא (מרכזי). תכונות אלה משתנות במהלך ההתנגשות המרכזית ולאורך התקדמותו באיירי הנפיץ אשר נמצא ברקע גם לאחר ההתנגשות. בסופה של ההתנגשות הסוליטון שואף להתייצב לתוך מצב סוליטוני אחר המתאים למצבו החדש. בנוסף ביצוע שינוים במדדים ההתחלתיים של פולס האיירי הניב (מיקום זמני התחלתי, פאזה, ועוצמה). טווח רחב של תוצאות, אשר הרחיב את הידע על אופי האינטראקציה.

האינטראקציה הופכת את סוגה מאינטראקציה קוהרנטית ללא קוהרנטית לפי התנאים המוכתבים במהלך השילוח עקב ההזזה הספקטרלית של מרכבי הספקטרום של האיירי על ידי תופעת הנפיצה. התוצאות של האינטראקציה מצביעות על כך שיש שינוים במדדים כגון התדר הנושא והעוצמה הכללית של הסוליטון. שינוים אלו ניתנים לאבחנה באמצעות שינוים במיקום הזמני והפאזה המצטברת בהתאם לשינוים שהוצגו קודם. מעבר לכך על פי תאוריית ההפרעות יתכנו גם שינוים עצמאיים (ללא תלות בשינוי התדר או העוצמה) של המיקום הזמני והפאזה המצטברת.

Table of Contents

1 Introduction

Bessel beams which were thought to be unique are diffractionless beams that have been theoretically introduced in 1987 [1] and later experimentally demonstrated in ref. [2]. However, it was not until recently that a new addition was introduced—Airy beams. An Airy wave packet was first introduced in 1979 [3] in the context of quantum mechanics. It was theoretically demonstrated that a nonspreading Airy wave packet is a solution to the Schrödinger equation for a particle with no external potential (free particle). While Bessel beams are a stationary solution, Airy beams have a remarkable ability to *freely accelerate* despite the absence of any external potential. However, Airy beams as well as Bessel beams require an infinite amount of energy to be realized. A solution to this predicament is the truncation of the beams that was first demonstrated on Bessel beams to utilize in the creation of non-diffracting beams [2]. It was only recently that the latter solution was applied to an Airy function to achieve non-diffracting Airy beams [4-6]. Despite truncation, Airy beams remain quite resilient to diffraction and stay self-similar over extended propagation distances. Furthermore, the characteristic acceleration is fully maintained. Truncated Airy beams are easily attainable by applying a cubic phase mask across a Gaussian beams in the Fourier plane. These unique attributes and experimental ease have sparked much interest surrounding Airy beams. As so, they have become the topic of research in many research groups. Spatially truncated Airy beams have been applied in creating curved plasma channels [7], particle clearing [8], plasmonic energy routing [9], and are capable of recovering from spatial obscurations due to their energy redistribution mechanism [10], making them useful for imaging in scattering media [11].

As it is known, the diffraction equation of light and temporal dispersive equation are isomorphic, therefore the attributes associated with spatial Airy beams can be directly translated to temporal Airy pulses. Similar to truncated Airy beams it is necessary to impose a cubic spectral phase on the pulse to achieve temporal truncated pulses. Such methods include shaping techniques [12] or propagation in cubic dispersive media (at the zero dispersion wavelengths) [13]. The resulting truncated pulse can achieve large propagation distances without succumbing to dispersion (in normal or anomalous dispersion media) which can lead to spatially and temporal confined pules or light bullets [12, 14]. Light bullets are an interesting combination of a truncated spatial Bessel beam and a truncated Airy temporal profile. When combined they create localized (confined) bundles of light both spatially and temporally. It is also possible to engineer Airy pulses to collide in time or space to achieve significantly high power enhancements [15].

Airy pulses and beams have also been experimented within nonlinear medias, particularly intensity dependent Kerr media. In such cases the Airy waveform is no longer an analytical solution to the Nonlinear Schrödinger equation (NLSE). Due, to the intensity distribution of the Airy beams and pulses the nonlinearity is strongest at the peak intensity and subsides with the minor lobes that follow. Therefore, the peak intensity experiences a greater amount of self-phase modulation (SPM) or self-focusing, offering a unique advantage when relatively low powers are applied to Airy beams. These allow for prolong propagation under such conditions [16]. As power is increased the formation and shedding of spatial solitons or multiple solitons can be observed [17]. Similarly the same phenomenon can be seen in the temporal domain [18]. Finally, creation and switching of Airy beams by parametric process was also demonstrated in a quasi-phased matched (QPM) media [19] along with spatiotemporal control in high-harmonic generation obtained by QPM structures [20].

Since Airy beams or pulses are not an analytical solution to the NLSE they are unable to maintain their shape during propagation in the presence of the optical potential created by the Kerr effect. However, a natural solution exists in the form of a soliton [21- 23] (soliton: a general term for a pulse that maintains its shape during propagation in nonlinear media). This stable solution maintains a balance between diffraction (dispersion—time domain) and self-focusing (SPM—time domain) which allows it to keep its intensity profile. It is a stationary solution and does not accelerate during propagation. Solitons have been extensively studied in both spatial [24] and temporal domains [25]. Research in to the latter was mainly out of interest for use in optical communications [26, 27]. Soliton “repeaterless” networks were first conjured by Hasegawa [28] while Mollenauer, Stolen and Gordon later demonstrated temporal soliton propagation [29]. In particular, soliton-soliton interactions were studied to investigate the effects that they have on soliton based communications. These interactions are categorized as either coherent [21, 30, 31] (interactions between successive bits) or incoherent [27, 32] (collisions between pulses of different wave division multiplexing (WDM) channel, due to group velocity mismatch).

Soliton perturbations were also extensively studied (i.e. fiber loss or local amplifications) [33-41]. These interactions (collisions and perturbations) establish the limiting factors for soliton-based optical communications [27].

The following thesis deals with the simulation of interactions between a weak truncated Airy pulse and soliton pulse in a single mode fiber (SMF) as the nonlinear medium. By keeping the Airy pulse weak, we preserve its linear characteristics and can treat the interaction as a perturbation of the stable soliton solution. Placing these pulses at proximity to one another, yet non-overlapping, and launching them at the same center frequency the Airy pulse can accelerate to interact with the soliton.

To better understand the interaction we vary the relative amplitude, phase and time separation of the Airy pulse relative to the soliton. This is based on insight from soliton-soliton and soliton-Continuous wave (CW) that show that these parameters influence the outcome of the interaction.

The results obtained show that the interaction is indeed influenced by the variation of these parameters. For example, an interesting result arises due to the variation of the time separation, which not only changes the collision distance. Such a variation also changes the duration of the interaction at collision point as will be shown later.

Chapter 2 introduces the NLSE equation, which is the governing equation for propagation. Being a second order differential equation the NLSE has only a few known analytical solutions and in most cases is solved by numerical methods. Chapter 3 elaborates on these methods, in particularly on the split step Fourier method (SSFM) and includes the considerations and limitations when it is employed. Chapter 4 is the implication of the SSFM in the investigation of the soliton-Airy interaction, and deals with the intricate details of the interaction. Finally, the work is concluded in the last chapter with a summary of my findings and possible future work.

2 Theoretical background.

The NLSE is the propagation equation that governs the behavior of optical pulse when the pulse widths are between ~10ns to 10fs. When optical pulses propagate inside a fiber they are influenced by both dispersion and nonlinear effects. These manifest themselves through changes in the pulse shape and spectrum. In this Chapter we will review the basic mechanism of both dispersion and the nonlinear phenomena and introduce the Airy and soliton pulses.

2.1 The pulse propagation equation.

To derive the pulse propagation equation we shall first recall and define a few equations and relations. Maxwell's equations (2.1-2.4) are the foundations of all the electromagnetic analysis and as such the propagation of optical fields in fibers [23].

$$\nabla \times \boldsymbol{E} = -\frac{\partial \boldsymbol{B}}{\partial t} \tag{2.1}$$

$$\nabla \times \boldsymbol{H} = \boldsymbol{J} + \frac{\partial \boldsymbol{D}}{\partial t} \tag{2.2}$$

$$\nabla \cdot \boldsymbol{D} = \rho \tag{2.3}$$

$$\nabla \cdot \boldsymbol{B} = \boldsymbol{0} \tag{2.4}$$

E-is the electric field, ***H***- the magnetic field, ***D***- electric flux, ***B***- magnetic flux, ***J***- the current density in the medium, $\boldsymbol{\rho}$- the free charge density. In optical fibers both ***J*** and $\boldsymbol{\rho}$ can be set to zero since there is no net charge and no currents present. The first relations are the relations between the flux densities ***D*** and ***B*** that are brought upon by the electric and magnetic field ***E*** and ***H*** respectively.

$$\boldsymbol{D} = \varepsilon_0 \boldsymbol{E} + \boldsymbol{P} \tag{2.5}$$

$$\boldsymbol{B} = \mu_0 \boldsymbol{H} + \boldsymbol{M} \tag{2.6}$$

ε_0-is the vacuum permittivity and μ_0- is the vacuum permeability. ***P*** and ***M*** are the induced electric and magnetic polarizations respectively. We focus on the electrically induced polarizations since in optical fiber ***M*** is equal to zero. The nonlinear wave equation for the electric field can now be attained by taking the curl of Eq. (2.1) and applying the rest of the Maxwell equations to arrive at equation (2.7).

$$\nabla^2 \boldsymbol{E} = -\frac{1}{c}\frac{\partial^2 \boldsymbol{E}}{\partial t^2} - \mu_0 \frac{\partial^2 \boldsymbol{P}}{\partial t^2} \tag{2.7}$$

When the frequency of the electric field is far from the resonance frequency of the medium, the response of ***P*** can be simply describe by:

$$\boldsymbol{P} = \varepsilon_0(\chi^{(1)}\boldsymbol{E} + \chi^{(2)}\boldsymbol{EE} + \chi^{(3)}\boldsymbol{EEE} + ...) \tag{2.8}$$

This is an expansion of the polarization that has been induced in the medium by an external electric filed: ε_0- is the vacuum permittivity and χ-is the electric susceptibility that describes the response of the bond electrons and molecules (nucleus) in the presence of an external electric field. To first order, ***P*** is linearly dependent on ***E*** and is a sufficient description as it is the main contribution. Although, when the intensity increases past a certain threshold (Electric field on the order of the binding atom [42]), higher order terms start to contribute and this is the source for nonlinear optics (NLO). The primary terms in NLO are the second and third order which relate to $\chi^{(2)}$ and $\chi^{(3)}$coefficients respectively in Eq. 2.8. When an electric field is substituted into equation(2.8), we receive a wide range of phenomena's from the combinatorial combinations [23, 43]. These are further grouped in to two categories; Phase matched processes and intensity driven processes [23, 43]. Phase matching implies that conditions are such that the carrier frequencies interact to produce new frequencies combinations. While in intensity driven process the carrier frequency of the field remains the same but influence is through changes in the refractive index. This induces a chirp that can create new frequencies (around the center frequency). Second harmonic generation (SHG) and third harmonic generation (THG) are two examples of a phased matched process in which two or three photons interact to produce new frequencies respectively. Examples of intensity driven processes include optical rectification ($\chi^{(2)}$-process) and self-focusing (spatial domain) or self-phase modulation (time domain) (SPM) ($\chi^{(3)}$-process). In our case the propagation is influenced by SPM since the conditions for phase matching are not present leading to a low probability for phase matching to occur. In addition, in most mediums, the $\chi^{(2)}$ processes have zero contributions due to symmetry properties [23, 42, 43] leaving the main contribution from the third order term as the lead term (Eq. 2.9).

$$\boldsymbol{P}_{NL}(\boldsymbol{r},t) = \varepsilon_0\chi^{(3)} \vdots \boldsymbol{E}(\boldsymbol{r},t)\boldsymbol{E}(\boldsymbol{r},t)\boldsymbol{E}(\boldsymbol{r},t) \tag{2.9}$$

SPM arises from the dependence of the refractive index on the intensity. This can be seen in the frequency domain with the following set of equations [23]:

$$\tilde{n}\left(\omega, |\boldsymbol{E}|^2\right) = n(\omega) + n_2 |\boldsymbol{E}|^2 \tag{2.10}$$

$$n(\omega) = 1 + \frac{1}{2}\mathrm{Re}\left[\tilde{\chi}^{(1)}(\omega)\right] \tag{2.11}$$

$$n_2 = \frac{3}{8}\mathrm{Re}\left(\chi^{(3)}_{XXXX}\right) \tag{2.12}$$

Equation 2.10 defines the refractive index in the presence of a high intensity electric field. In Eq. 2.10, n_2 is a measurement of the fiber nonlinearity defined by Eq. 2.12.

We split the polarization to a linear and nonlinear contribution (Eq.2.13).

$$\boldsymbol{P}(\boldsymbol{r},t) = \boldsymbol{P}_L(\boldsymbol{r},t) + \boldsymbol{P}_{NL}(\boldsymbol{r},t) \tag{2.13}$$

Substituting this in to Eq. (2.7) we arrive at:

$$\nabla \boldsymbol{E}^2 - \frac{1}{c}\frac{\partial^2 \boldsymbol{E}}{\partial t^2} = \mu_0 \frac{\partial^2 \boldsymbol{P}_L}{\partial t^2} + \mu_0 \frac{\partial^2 \boldsymbol{P}_{NL}}{\partial t^2} \tag{2.14}$$

Prior to solving Eq. 2.14 we will require to make several simplifying assumptions. First, $\boldsymbol{P}_{NL}$ is treated as a small perturbation to $\boldsymbol{P}_L$, since in practice it is on the order of 10^{-6} [23]. Second, the optical field is assumed to maintain its polarization so that the scalar approach is valid. Third the pulse spectrum is assumed to have a narrow spectral width ($\Delta\omega/\omega_0 \ll 1$). For example $\omega_0 \sim 10^{15}$, this will coincide with pulse widths as short as 0.1ps. Lastly, we will assume that the medium's nonlinear response is instantaneous. (The instantaneous response of the medium assumes that the contributions are from the electrons and not the molecular vibrations that result in the Raman effect. We shall not concern ourselves with the Raman contribution and thus are limited to pulses widths that are larger than 1ps). A solution can now be presented as a multiplication of three terms [23].

$$\boldsymbol{E}(\boldsymbol{r},t) = \frac{1}{2}\hat{x}\left\{F(x,y)A(z,t)\exp(i\beta_0 z - \omega_0 t) + c.c\right\} \tag{2.15}$$

Without loss of generality we assume that the solution $\boldsymbol{E}$ is in the x direction. The function $F(x,y)$ dictates spatial dependence of the field and incorporates the geometry of the medium. For example in an optical fiber the fields' first mode (fundamental mode) that develops due to the boundary conditions has an intensity distribution similar to a Gaussian intensity profile. The spatial dependence is found by finding the eigenvalues for $F(x, y)$ with a given choice of coordinate presentation [23] when Eq. (2.15) is substitute in to Eq. (2.14). However, the complete derivation requires the transitions between the time domain and the frequency domain where significant simplifications are gained. We shall not proceed with the full derivation of the spatial dependence but will proceed under the assumption that the fiber is a single mode fiber (having only the transverse electric mode). Our main concern is the behavior of the temporal envelope *A(z,t)* of the field during propagation along the z direction. Therefore, Eq. 2.16 is also the consequence of the latter substitution with the added assumption that regards the envelope as slowly varying with respect to *z* $\left(\left|\partial^2 A/\partial z^2\right| << \beta_0^2 \left|A\right|\right)$, where β_0-is the wave number. This resulting equation is usually referred to as Nonlinear Schrödinger Equation (NLSE).

$$\frac{\partial A}{\partial z} + \beta_1 \frac{\partial A}{\partial t} + i\beta_2 \frac{\partial^2 A}{\partial t^2} + \frac{\alpha}{2} A = i\gamma \left|A\right|^2 A \tag{2.16}$$

The first term is the differentiation of the *A(z,t)* with respect to *z*. The next two terms from the left, are the consequence of the expansion of the wave number β which is frequency dependent.

$$\beta(\omega) = \beta_0 + (\omega - \omega_0)\beta_1 + \frac{1}{2}(\omega - \omega_0)^2 \beta_2 + \frac{1}{6}(\omega - \omega_0)^3 \beta_3 \tag{2.17}$$

β_1-represents the group velocity of the pulse $v_g = 1/\beta_1$, β_2 - is the quadratic dispersion coefficient (GVD: Group velocity dispersion). The fourth term is the loss or gain term determined by the sign of α. Last is the nonlinear term arising from SPM, as pointed out earlier the refractive index is dependent on the electric field according to this relation: $n = n_0 + n_2 \left|E\right|^2$,which is known as the Kerr effect; γ is defined by Eq. (2.13):

$$\gamma = \frac{n_2 \omega_0}{c A_{eff}} \tag{2.18}$$

A_{eff} -parameter is known as the effective are of the fiber mode. It relates the mode distribution to the size of the core. An example would be a Gaussian distribution; $A_{eff} = \pi w^2$, *w*- is the width of the Gaussian (depending on how the Gaussian is defined).

2.2 The Dispersion phenomena.

In this section we will discuss in detail the effects of group velocity dispersion (GVD) by treating the optical fiber as a linear optical medium. In such a case the nonlinear term in Eq. (2.16) is neglected. To simplify things further we will also assume a loss-less fiber. However first we must set the criteria when a medium can be considered linear.

2.2.1 Propagation regimes

Representation of Eq. (2.16) in the retarded time frame allows for further simplifications with the following transformation $T = t - z\beta_1 = t - z/v_g$ [23]:

$$\frac{\partial A}{\partial z} + i\beta_2 \frac{\partial^2 A}{\partial T^2} + \frac{\alpha}{2} A = i\gamma |A|^2 A \tag{2.19}$$

T – is the time in the retarded time frame moving at group velocity.

To determine the propagation regions it is necessary for us introduce the normalized form of Eq. (2.19), which will allow for the definition of the characteristic lengths for the dispersion and the nonlinear phenomena's and thus establishing the criteria for pulse propagation regions.

Defining Eq. (2.20) where $\tau = T/T_0$, T_0 is the initial pulse width and P_0 is the initial power, we can substitute Eq. (2.20) in to Eq. (2.19) to arrive at Eq. (2.21).

$$A(z,\tau) = \sqrt{P_0}\exp(-\alpha z/2) U(z,\tau) \tag{2.20}$$

$$i\frac{\partial U}{\partial z} = \frac{\mathrm{sgn}(\beta_2)}{2L_D}\frac{\partial^2 U}{\partial \tau^2} - \frac{\exp(-\alpha z)}{L_{NL}} |U|^2 U \tag{2.21}$$

sgn(β_2)- is the sign function and has the values of ±1 depending on the sign of β_2.

L_D and L_{NL} (Eq.(2.22)) are the characteristics lengths for the dispersion and nonlinear phenomena's respectively and they offer a scale for which the effect of the dispersion and nonlinear effects becomes relevant. The physical interpretation of L_{NL} is the distance at which the π phase shift contribution is attained through SPM, while after L_D a Gaussian pulse would have accumulated an increase in duration by $\sqrt{2}$. We are now in a position to define the propagation regimes.

$$L_D = \frac{T_0^2}{|\beta_2|} \qquad L_{NL} = \frac{1}{\gamma P_0} \tag{2.22}$$

1. $L_D \approx L_{NL} < L$ are of the same magnitude and both are smaller than L, neither of terms in Eq. (2.21) can be neglected and both will influence the pulse during propagation.
2. $L_D < L < L_{NL}$ in this case the nonlinear term in Eq. 2.21 can be neglected and the pulse evolution is governed by GVD only.
3. $L_{NL} < L < L_D$ for this case the dispersion term is negligible and the pulse evolution is governed by nonlinear term.

2.2.2 Dispersion- induced pulse broadening

Assume we are in condition 1, then Eq. (2.21) can be simplified to:

$$i\frac{\partial U(z,T)}{\partial z} = \frac{\beta_2}{2}\frac{\partial^2 U(z,T)}{\partial T^2} \tag{2.23}$$

To solve Eq. (2.23) we transfer over to the Fourier domain were Eq. (2.23) has a simpler form;

$$i\frac{\partial \tilde{U}(z,\omega)}{\partial z} = -\frac{\beta_2}{2}\omega^2\tilde{U}(z,\omega) \tag{2.24}$$

$$\tilde{U}(z,\omega) = \tilde{U}(0,\omega)\exp\left(\frac{i}{2}\beta_2\omega^2 z\right) \tag{2.25}$$

Solving Eq. (2.24) leads to the solution Eq. (2.25) which states that any initial condition can be propagated in the frequency domain to a predetermined distance by a multiplication of an exponential phase term that is both frequency and distance depended. An analysis of Eq. (2.25) shows that each spectral component receives a change in phase proportional to its frequency at a given distance. This however does not change the power spectrum but does alter the pulse temporal profile. Therefore, we can propagate any arbitrary initial condition by a transformation to the frequency domain, carry out the propagation and return by taking the inverse Fourier transform Eq.(2.26).

$$U(z,t) = \frac{1}{2\pi}\int_{-\infty}^{\infty}\tilde{U}(0,\omega)\exp\left(\frac{i}{2}\beta_2\omega^2 z - i\omega t\right)d\omega \tag{2.26}$$

Figure 2.1 shows an example of a broadening Gaussian pulse (initial condition given by Eq. (2.27) without any spectral alterations during propagation.

$$U(0,T) = \exp\left(-\frac{T^2}{2T_0^2}\right) \tag{2.27}$$

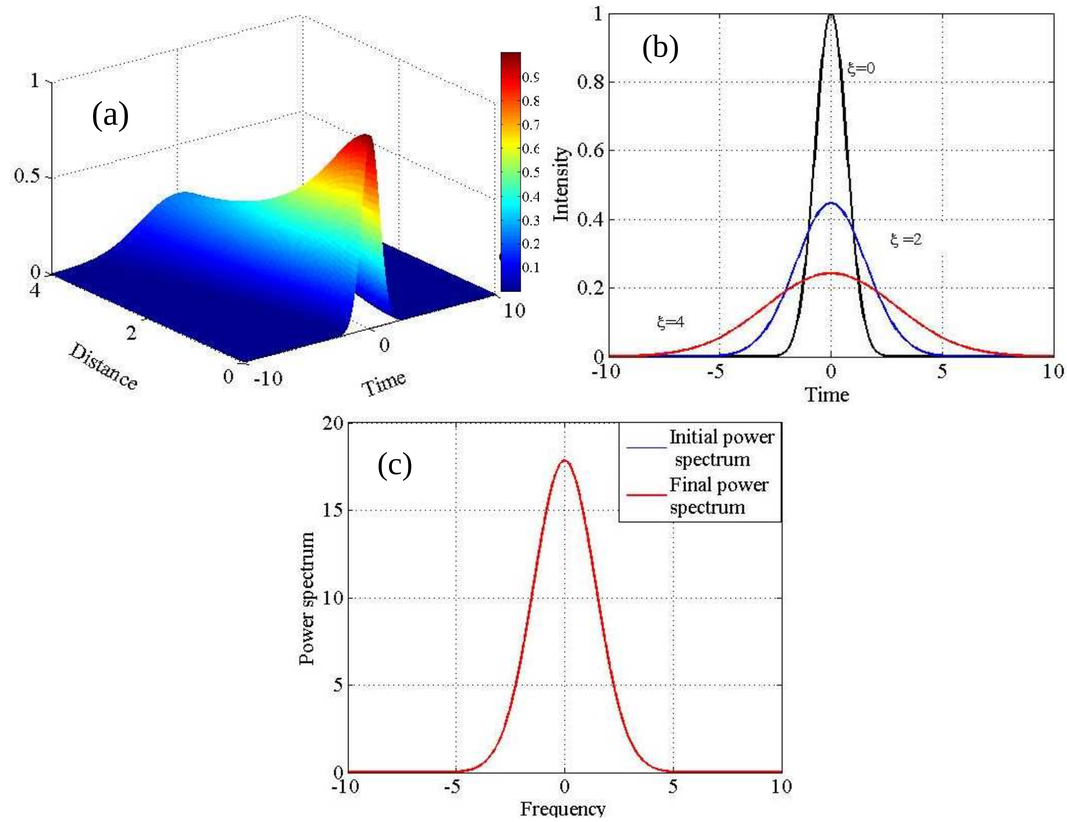

Fig. 2.1. (a) The evolution of Gaussian pulse with an initial amplitude of 1, initial width of 1, in a loss less fiber and no nonlinear effects.(b) The broaden Gaussian pulse at different dispersion lengths ($L_D=1$),(c) Initial and final power spectrum.

Dispersion can either compress or broaden a pulse depending on the sign of the product between the quadratic dispersion (β_2) and the chirp. The chirp is defined as the instantaneous frequency across the pulse, and is mathematically defined as; $\delta\omega = -\partial\phi/\partial T$, where ϕ is the argument of the temporal phase term of the pulse. In addition, β_2 can either positive or negative. When β_2 is positive, this is known as normal-dispersion, were low frequency components travel faster than high frequency components. While when β_2 is negative the opposite is true and this is known as anomalous dispersion. When the medium has anomalous dispersion it is possible to achieved optical solitons with dispersion balancing the spectrum generated by SPM (both produce a chirp at the same magnitude but opposite in sign).

2.3 Airy

Airy wavepackets having been first theoretically suggested by Berry and Balazs [3], with little interest devoted till recently when Christodoulides *et. al.* demonstrated [4-6] Airy beams by truncation of the Airy tail. This sparked much interest among many research groups (see the section 1-Introducation). In this section we will review in brief Airy beams and follow up with Airy pulses after showing the analogy between the dispersion equation and diffraction equation.

2.3.1 Airy function

Before moving on to Airy beams in space, we review in brief the Airy function and the truncation procedure. The Airy function has many mathematical definitions [44], one integral presentation is:

$$Airy(x) = \frac{1}{\pi}\int_0^\infty \cos\left(\frac{t^3}{3} + xt\right)dt\ /; \mathrm{Im}(x) == 0 \tag{2.28}$$

Figure 2.3a shows a plot of an Airy function and Fig. 2.3b is of a truncated Airy beam:

$$Airy_{Trun.}(x) = Airy(x)\exp(ax)\ /; a > 0 \tag{2.29}$$

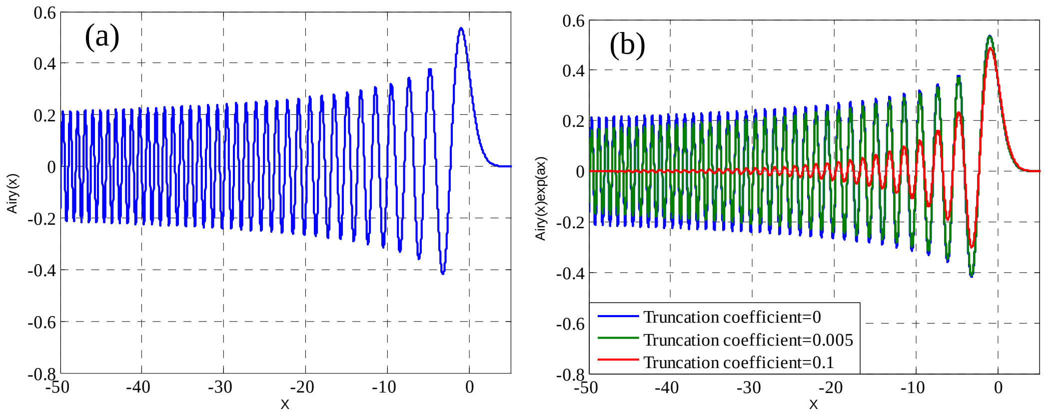

Fig.. 2.3. (a) Airy function,(b) Truncated Airy function with different truncations.

The zeros of the Airy function along with other properties can be found in [44.]

2.3.2 Airy beams in space

An initial condition of a truncated Airy (in normalized units) of the form:

$$U(s,\zeta=0)=\mathrm{Airy}(s)\exp(as) \tag{2.30}$$

Will diffract according to [2]:

$$\begin{aligned}U(s,\xi)=\mathrm{Airy}[s-(\xi/2)^2+ia\xi]\exp(as-(a\xi^2/2)-i(\xi^3/12)\\+i(a^2\xi/2)+i(\xi s/2))\end{aligned} \tag{2.31}$$

Where *s* is the normalized transverse coordinate $\left(s=x/x_0\right)$ and ξ is the normalized propagation distance $\left(z=2\pi n/\lambda_0\right)$. When setting *a*=0 one receives the theoretical non-diffracting Airy beam (is such a case the energy of the beam, $\int_{-\infty}^{\infty}\left|U\left(s,\xi\right)\right|^2 ds$ does not converged). The origin of the Airy's parabolic translation is in its argument. When looking at constant plains, $s-\left(\xi/2\right)^2=constant$ the relation between *s* and ξ is quadratic.

2.3.3 Airy pulses in time

The mathematical equations of diffraction (Eq.(2.32)) and dispersion (Eq.(2.33)) are isomorphic [23].With a simple translation between $k\leftrightarrow-\beta_2$ and $x\leftrightarrow T$ we can move between the two domains.

$$i\frac{\partial U\left(x,z\right)}{\partial z}k+\frac{1}{2}\frac{\partial^2 U\left(x,z\right)}{\partial x^2}=0 \tag{2.32}$$

$$i\frac{\partial U(T,z)}{\partial z}-\frac{\beta_2}{2}\frac{\partial^2 U(T,z)}{\partial T^2}=0 \tag{2.33}$$

To transfer equations (2.30) and (2.31) to the time domain we make the following substitution:

$$s\to\frac{T}{T_0};\qquad \xi\to\frac{z\beta_2}{T_0^2} \tag{2.34}$$

Equations (2.35) and (2.36) are there equivalence in the time domain respectively.

$$U(T,z=0)=\mathrm{Airy}(\frac{T}{T_0})\exp(\frac{aT}{T_0})\exp(i\frac{T\nu}{T_0}) \tag{2.35}$$

$$
\begin{aligned}
U(T,z) = \mathrm{Airy}[\frac{T}{T_0} - \left(\frac{z\beta_2}{2T_0^2}\right)^2 - \nu\frac{z\beta_2}{T_0^2} + ia\frac{z\beta_2}{T_0^2}]\exp[a\frac{T}{T_0} - (\frac{a}{2}\left(\frac{z\beta_2}{T_0^2}\right)^2) - a\nu\frac{z\beta_2}{T_0^2}]\times \\
\exp[i(-\frac{1}{12}\left(\frac{z\beta_2}{T_0^2}\right)^3 + \frac{1}{2}(a^2 - \nu^2 + \frac{T}{T_0})\left(\frac{z\beta_2}{T_0^2}\right) + \nu\frac{T}{T_0} - (\frac{\nu}{2}\left(\frac{z\beta_2}{T_0^2}\right)^2))]
\end{aligned} \tag{2.36}
$$

In Eq. (2.35) and (2.36) we added an initial velocity parameter ν [3] that causes a shift in the carrier frequency and thus contributes an additional term to the translation of the peak in time as $T/T_0 = \nu\, z\beta_2/T_0^2 + \left(z\beta_2/2T_0^2\right)^2$. (In the diffraction analogy, the velocity term is a linear spatial phase tilt). A plot of exemplary dispersed Airy pulses (Eq.(2.36)) with different initial conditions is shown in figure 2.4.

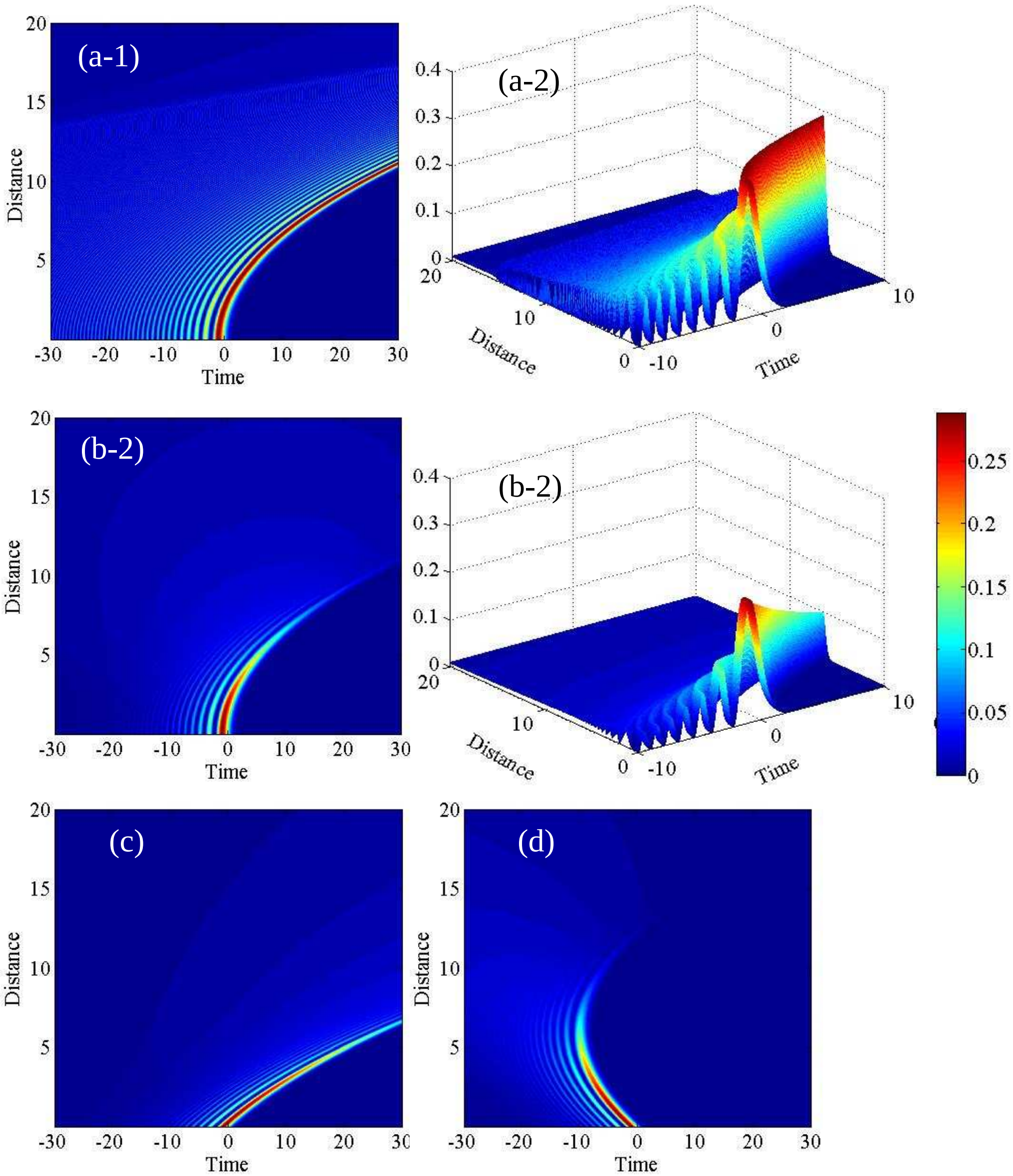

Fig. 2.4. Airy intensity distribution when propagating with in a dispersion medium,having no loss. Initial conditions are: initial width of 1 and amplitude of 1,(a) Non truncated Airy, Truncated Airy with a= 0.05 (b) ν=0, (c) ν=3 and (d) ν= -3.

From figure 2.4 we can see that Airy pulses maintain their shape while propagating over extended regions. For comparison, Gaussian pulses can travel $\sqrt{3}\,L_D$ (where L_D is the dispersion length) before the peak intensity is reduced by half, whereas an Airy pulse can travel several dispersion lengths; for example, an Airy pulse with *0.05 (0.005)* truncation coefficient can propagate $5.5L_D$ ($16.7\ L_D$) before the peak intensity is reduced by half (Fig. 2.5). The increase in dispersion lengths for larger truncation is explained by the fact that as we increase the truncation coefficient we further broaden the pulse in positive side of the axis thus the wider the pulse the less it disperses.

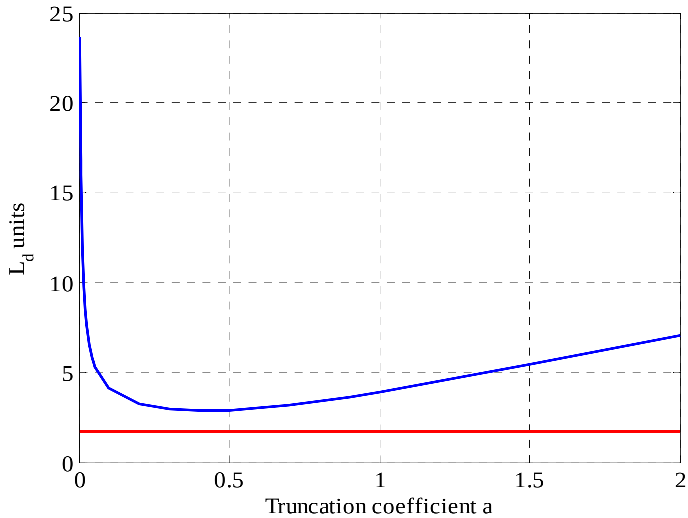

Fig. 2.5. Distance propagated (normalized to the characteristic dispersion length ,L_D)
to reach half power of the primary peak for a Truncated Airy with different truncation coefficients (blue line). The red line is the distance required for a Gaussian to reach half peak power.

2.4 The Nonlinear phenomena

The nonlinear phenomena manifest itself through the dependence of the refractive index on the intensity of the electric field. This causes self-phase modulation that leads to the broadening of the spectrum of optical pulses. To focus on the nonlinear phenomena in the absence of dispersion, we can set β_2 =0. Though, in practice if the power and pulse width satisfy $L_D >> L_{NL}$, we would be in the nonlinear propagation regime.

2.4.1 SPM-Induced Spectral broadening

Assuming that such conditions are met:

$$\frac{\partial U}{\partial z} = \frac{i \exp(-\alpha z)}{L_{NL}} |U|^2 U \tag{2.37}$$

To solve Eq.(2.37), we substitute $U = V \exp(i\phi_{NL})$ as a probable solution. Therefore, separating to its real and imaginary parts we get:

$$\frac{\partial V}{\partial z} = 0; \quad \frac{\partial \phi_{NL}}{\partial z} = \frac{\exp(-\alpha z)}{L_{NL}} V^2; \tag{2.38}$$

Form Eq. (2.38) we deduce that the amplitude V is independent of z, thus, the equation for the phase can be analytical integrated:

$$\begin{aligned} \phi_{NL}(z,T) &= |U(0,T)|^2 (L_{eff} / L_{NL}) \\ Leff &= [1 - \exp(-\alpha z)] / \alpha \end{aligned} \tag{2.39}$$

Equation 2.39 reviles that during propagation the pulse shape remains unaltered (Fig. 2.2a), and the SPM gives rise to an intensity-dependent phase shift. The phase profile would be that of the pulse shape after L_{NL} in a lossless fiber (Fig. 2.2b).

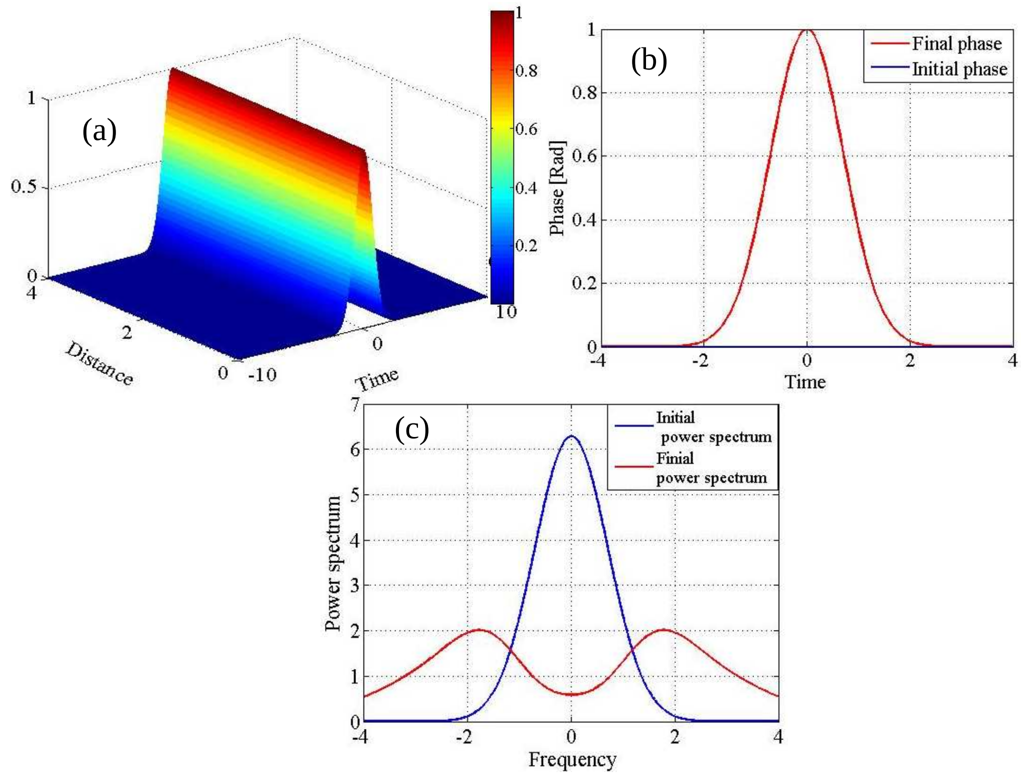

Fig. 2.2. (a) A Gaussian pulse maintains its shape during propagation in a nonlinear fiber with initial amplitude of 1 for $4L_{NL}$. (b) A Gaussian induced phase profile at the end of propagation (c) Initial and final power spectrum showing the induced chirp across the spectrum.

2.4.2 Cross phase modulation

When two fields with different or same frequency co-propagate in a SMF they can interact through the nonlinear term. When $A = A_1 + A_2$ is inserted into Eq. (2.19) new terms are produced in each equation [23, 42, and 43]:

$$\begin{aligned} &\frac{\partial A_1}{\partial z} + + i\beta_2 \frac{\partial^2 A_1}{\partial T^2} + \frac{\alpha}{2} A_1 = \underbrace{i\gamma |A_1|^2 A_1}_{SPM} + \underbrace{2i\gamma |A_2|^2 A_1}_{XPM} \\ &\frac{\partial A_2}{\partial z} + i\beta_2 \frac{\partial^2 A_2}{\partial T^2} + \frac{\alpha}{2} A_2 = i\gamma |A_2|^2 A_2 + 2i\gamma |A_1|^2 A_2 \end{aligned} \tag{2.40}$$

In the Eq. (2.40) we ignored terms that oscillate at the new frequencies $2\Omega_1 - \Omega_2$ or $2\Omega_2 - \Omega_1$ since they require phase matching in order to produce any significant contribution, thus we are left with the cross-phase modulation (XPM). Due to the presence of two fields the refractive index is now influenced by the intensity from both fields. Each field now produces a nonlinear phase shift proportional to its intensity on the other filed.

2.5 The Soliton Pulse

Solitons are eigen-functions of the NLSE in anomalous dispersion media, brought about by the balance between dispersion and self-phase focusing due to the Kerr effect $(L_D = L_{NL} \Rightarrow |\beta_2|/T_0^2 = 1/\gamma P_0)$. It was first analytically derived by V.E Zakharov and A.B. Shabat that showed that the soliton is a solution to the NLSE with the aid of the Inverse Scattering Method (ISM) [21]. The first order soliton solution has the canonical form [6, 15] (with units):

$$U(T,z) = A\,\mathrm{sech}((T - T_{soliton})/T_0)\exp(i\,z\beta_2/T_0^2) \qquad (2.41)$$

$T_{soliton}$- Initial time position of the soliton.

Equation (2.41) states that the soliton maintains its shape (Fig. 2.6a) and only acquires a cumulative phase that is linearly dependent on the propagation distance (Fig. 2.6b). Solitons can also arise in the presence of an arbitrary pulse shape with an energy surplus with respect to the soliton condition [23, 26]. The formation of the soliton evolves during the propagation with the pulse shedding off excess energy to settle in a soliton state.

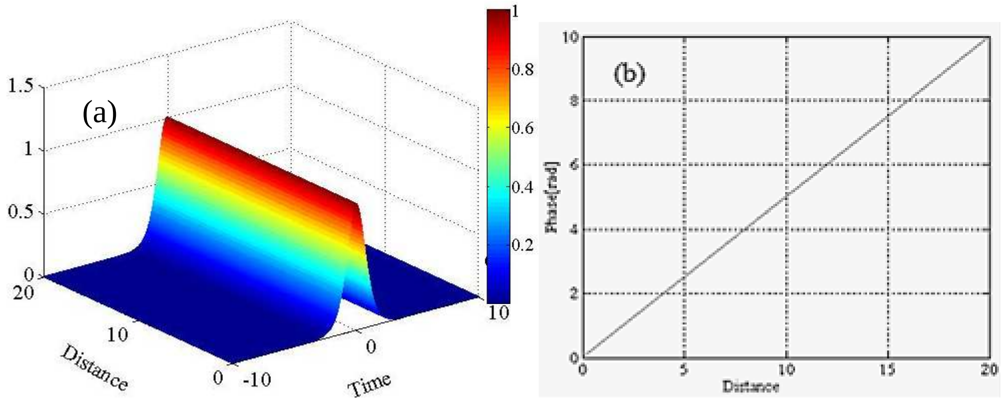

Fig.. 2.6. (a) Soliton propagation with L_D=L_{NL}=1,(b) a linearly accumulated phase during propagation.

3 Numerical Simulation for pulse propagation.

The Nonlinear Schrödinger Equation (NLSE) is a nonlinear partial differential equation that does not generally lend itself to analytical solutions except for some cases in which the inverse scattering method can be employed [21]. Therefore numerical approaches are necessary for solving the NLSE. These are classified into two broad groups, 1) finite-difference methods and 2) pseudospectral methods [23]. The method used extensively is the pseudospectral split-step Fourier method (SSFM). Pseudospectral methods are generally faster by 2 orders of magnitude while achieving the same accuracy.

3.1 Introduction to the Split Step Fourier method.

The NLSE (Eq. (2.19)) can be expresses as the sum of two differential operators [23].

$$\frac{\partial A}{\partial z} = (\hat{D} + \hat{N})A \tag{3.1}$$

In Eq. 3.1 $\hat{D}$ is the linear operator the accounts for dispersion and loss (gain), $\hat{N}$ is a nonlinear operator that governs the nonlinear effects in the fiber during propagation.

$$\hat{D} = -\frac{i\beta_2}{2}\frac{\partial^2}{\partial T^2} + \frac{\beta_3}{6}\frac{\partial^3}{\partial T^3} - \frac{\alpha}{2} \tag{3.2}$$

$$\hat{N} = i\gamma |A|^2 \tag{3.3}$$

These operators act together continuously and simultaneously on the pulse during propagation. When applying the split-step Fourier method an assumption is made that over a small distance *h* these two operators are independent on one another. Propagation for *z* to *z+h* is carried out by applying the following expression.

$$A(z+h,T) \approx \exp(h\hat{D})\exp(h\hat{N})A(z,T) \tag{3.4}$$

$\hat{D}$ can be more conveniently applied in the Fourier domain. Therefore, using the Fourier identity $d^n f(t)/dt^n = (i\omega) f(\omega)$, $\hat{D}$ is transformed to the Fourier domain where its application is much more practical.

$$\hat{D} = \frac{i\omega^2\beta_2}{2} - \frac{i\omega^2\beta_3}{6} - \frac{\alpha}{2} \tag{3.5}$$

Propagation along the fiber is carried out by consecutively operating on each segment with $\hat{N}$ and then $\hat{D}$ keeping the order, due to the non-commuting nature between the operators, till the whole fiber is complete. However, the SSFM ignores the non-commuting nature of the operators [23]. Therefore, simplifications and improvements in accuracy of the SSFM simulation can be implemented. For example one variation to improve the accuracy is to apply the dispersion operator to the first half of the segment then operate on the full segment with the nonlinear operator and complete the second half with another application of the dispersion operator for the remaining segment.

$$A(z+h,T) \approx \exp\left(\frac{h}{2}\hat{D}\right)\exp\left(\int_{z}^{z+h} N(z')dz'\right)\exp\left(\frac{h}{2}\hat{D}\right)A(z,T) \tag{3.6}$$

The advantage gained through this variation is that the nonlinear contribution is not taken at the boundaries but integrated over the segment. However, if the step size is small this can be taken to be $\exp(h\hat{N})$. The latter method is known as the symmetrized SSFM and in this case the leading error term is third order in the step size *h* [23].

3.2 The Algorithm.

Based on the last variation our algorithm is developed:

- ❖ Step 1: Divide the fiber in to segments (Fig. 3.1).
- ❖ Step 2: Split the segment in two equal parts.
- ❖ Step 3: Operate on the first half with the dispersion operator.
- ❖ Step 4: Operate on the entire segment with the nonlinear operator.
- ❖ Step 5: Operate on the second half with the dispersion operator.
- ❖ Step 6: Repeat steps two through five for the adjacent segment with the result obtained from the previous segments.

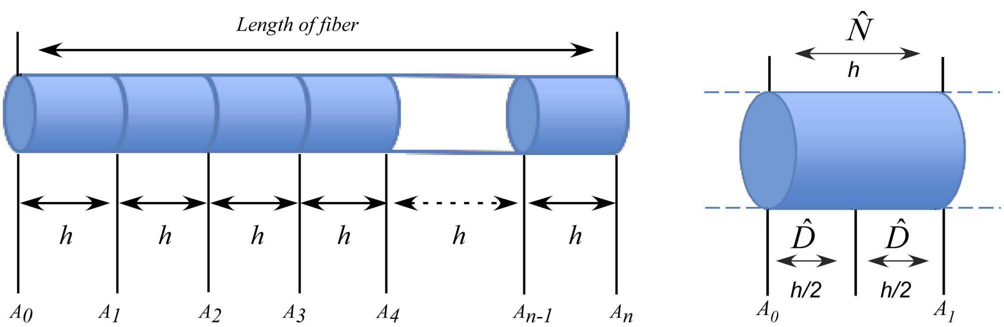

Fig. 3.1. Segmentation of the fiber (left). Separation of a segment into two parts for application of the dispersion operator (right).

3.3 Considerations and Limitations.

There are some considerations and limitations that must be addressed prior to the application of SSFM. The prominent one is the step size h (the length of a fiber segment). To acquire a reasonable accuracy we aspire that h would be at least two orders of magnitude less than the dominant phenomena governing the propagation. However, the optimum choice h depends on the complexity of the problem at hand. For example, a pulse can compress or broaden by dispersion, continuously changing L_D. Therefore h must be adjusted accordingly if L_D is reduced during propagation to maintain reasonable accuracy. To be able to take into account such scenarios we take h to be at least 3 orders of magnitude smaller than the dominant initial characteristic length.

Another consideration is due to the repetitive nature of the Fourier transform when the pulse energy reaches the ends of the time window energy gets feedback (cycled back from end to the other) into the pulse and does decay creating unreliable results. This can be overcome by simply making the time window large enough, thus confining the pulse in the time window over the propagation range. The latter method although very practical in most cases and simple has a limiting factor. The drawback is that this requires large vectors resulting in more processing time and requires more memory. A more advance solution is the introduction of limiting window that when the pulse reaches the ends of the time window the energy is absorbed preventing the feedback. In this case, care must be taken so a gradual decay of the pulse will be carried out and not an abrupt cutoff of the pulse which will also generate a reflection due to an abrupt transition. To prevent this from happening the criteria to keep in mind is the rate of temporal spread with respect to the step size, which needs to ensure that the amount of temporal spread takes place over a few steps. This is also true in the frequency domain and a delicate balance must be kept. Last, when dealing with pulses that are less than 5ps, further terms must be taken into account in the operators. These terms are added to the nonlinear operator and are caused by Raman scattering, though are not present in our simulation scenario [23].

4 Airy-Soliton interactions

Our initial intention was to demonstrate an overtake of a Gaussian pulse by utilizing the parabolic trajectory of an Airy pulse. Though, with our chosen configuration, the broadening rate of the Gaussian was faster than that of the Airy's acceleration. Thus, the Gaussian pulse engulfed the Airy pulse and the two pulses propagate through one another while experiencing interference.

However, a solution presented it self in the form of a soliton pulse. Solitons do not broaden during propagation and are a stationary but require a nonlinear medium to form. This requirement limits us to launching a weak Airy pulse in order to stay in the linear propagation regime. This intern raises an interesting question on the nature of the interaction, can a soliton pulse act as an optical potential barrier for the accelerating Airy pulse [45] (as an event horizon) or as a shepherding pulse [46]? Our initial trials did not indicate this, however, we do believe that this warrants further research, particularly with a soliton that is much more intense (shorter pulse width) which will increase the depth of the optical potential well.

Seeing that the soliton was experiencing changes we continued on the path of introducing an Airy pulse as a perturbation to the soliton pulse. We found preferable for sake of calculations and analysis to continue with dimensionless equations and operators and assume a lossless (*α=0*) fiber for the Airy pulse (Eq.(4.1)) perturbation of a soliton pulse (Eq.(4.2)).

$$\begin{aligned} u(\tau,\xi) = \mathrm{Airy}[\tau-(\xi/2)^2+ia\xi]\exp(a\tau-(a\xi^2/2)-i(\xi^3/12) \\ +i(a^2\xi/2)+i(\xi\tau/2)) \end{aligned} \tag{4.1}$$

$$u_s(\tau,\xi) = a\,\mathrm{sech}(a\tau)\exp(ia^2 z) \tag{4.2}$$

The unique ballistic propagation feature of the Airy pulse gives it the ability to accelerate or decelerate (depending on the tail direction) and allows for interactions (collisions) between pulses having the same center frequency. By positioning the soliton pulse along the ballistic path of the Airy they can cross and interact with one another.

These interactions are demonstrated through numerical simulations via the Split Step Fourier Method (SSFM) with a time window of 1300 time units divided to 32768 sampling points, and propagated to a distance of 100 Soliton periods (157L_D units, where L_D=1 in our normalized NLSE Eq.) with 1500 output inspection distances (not to be confused with the SSFM simulation step size which is less than one thousandth of L_D). Insight from the well-known soliton-soliton [21, 23, 29, 30] and soliton-continuous wave (CW) [33, 36, 37] interactions are applied to better understand the observed phenomena. It is known that relative phase, amplitude (or total energy), the initial separation and frequency offset (difference in group velocities) play a role in the outcome of the interaction; thus in our simulations we vary these initial parameters of the perturbing Airy pulse to take them into consideration. Consequently the launched initial conditions are Eq. (4.3) (Fig. 4.1a, with figure 4.2 showing individual propagation intensity plots):

$$u(\xi = 0, \tau) = \sec h\left(\tau\right) + rAiry(\tau - \tau_0)\exp(a\tau)\exp\left(i\theta\right) \tag{4.3}$$

The varied parameters in Eq. (4.3) are the amplitude ratio r between the Airy pulse and the soliton (normalized), the initial Airy time position τ_0 with respect to the soliton (launched at zero), and the relative phase θ of the Airy pulse. We choose r such that at the point of collision the intensity ratios between the accelerated Airy lobe and the soliton will be *8*, *4*, *2*, *1* and *0.5* percent (note that the Airy peak intensity at collision is already attenuated with respect to launched conditions on account of the truncation and dispersive propagation). These low Airy interference values ensure that the Airy will propagate in the quasi-linear regime and can be treated as a perturbation of the soliton [34]. The minimal time separation of $\tau_0=-6$ is chosen to achieve at least a -*30*dB dip between the Airy and soliton at our time sampling (Fig. 4.1b), to ensure essenitially no initial overlap. We also choose a small enough truncation coefficient (a=0.005), which guarantees that the peak collision intensity of the Airy launched at our largest separation ($\tau_0=-10$) will not be less than *95%* of that launched at the smallest separation ($\tau_0=-6$) for every chosen launched amplitude. Hence all the Airy pulses have the same energy for a given r value and only a small variation in peak intensity at the point of collision.

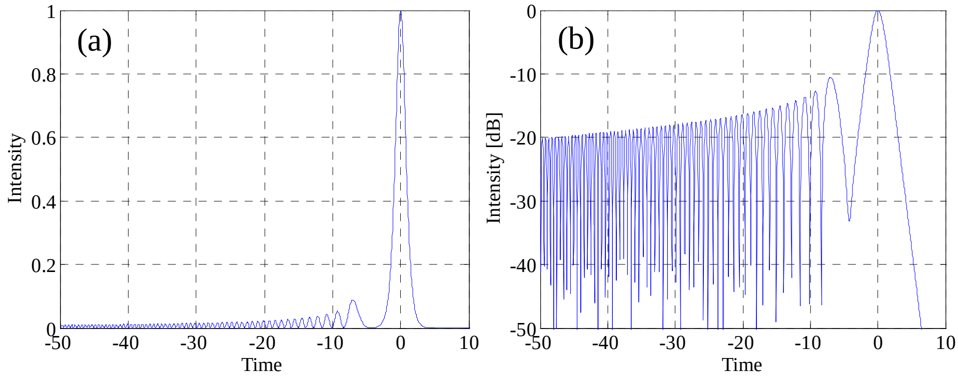

Fig. 4.1. Exemplary initial launch conditions composed of both the Airy ($a=0.005$, 8% intensity at collision, $\tau_0=-6$) and the normalized soliton. (a) linear scale, (b) dB scale (the variation in dip values is an artifact of the sampling).

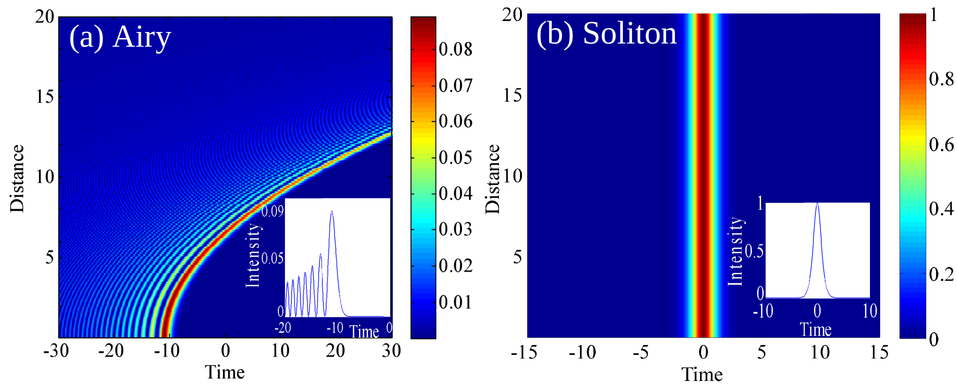

Fig. 4.2. Intensity plots for propagation of (a) a truncated Airy pulse ($a=0.005$), and (b) a normalized soliton both to $20\ L_D$. Insets show launched intensity distributions.

4.1 Simulations Results

Exemplary Airy-Soliton interactions are shown in Fig. 4.3, launched at a time separation of 10 time units ($\tau_0=-10$) and an intensity ratio of *8%* for two relative phases (0 and π). The propagating Airy decelerates (wavefront moves to later time) to collide with the trailing soliton pulse. The collision distance is given by:

$$\xi = \sqrt{4(\tau_{soliton} - \tau_0 + \tau_{peak\ off\ set})} \tag{4.4}$$

where $\tau_{soliton}$ is the Soliton time position (in our case $\tau_{soliton}=0$) and τ_{peak} offset is the offset of the main Airy peak with respect to the Airy delay time τ_0 ($\tau_{\text{peak offset}}$ is numerically calculated for a given truncation, e.g. $\tau_{peak\,offset} \approx 1.014$ for a=0.005.

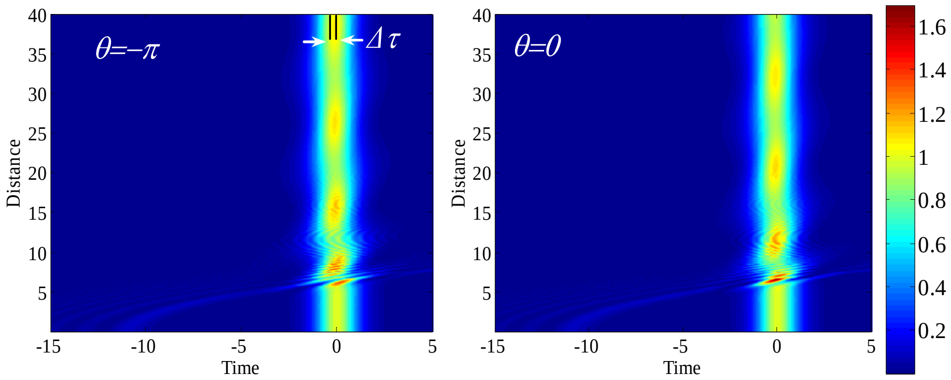

Fig.4.3 Airy-soliton interactions with an initial separation of 10 and intensity ratio of 8% at collision for two phases. (a) $\theta=-\pi$, (b) $\theta=0$

The interaction can be separated to two regimes of interest: the primary collision region between the pulses (occurring at approximately $3<\xi<15$, for our selected initial time separations), responsible for the main variation in the fundamental soliton parameters of phase, amplitude, frequency and time position [34], and a relaxation region accompanied by continuous interaction with the dispersed Airy tail (occurring at $\xi>15$). During the primary collision ($3<\xi<15$) both pulses lose their identities and cannot be distinguished [37] due to interference throughout the collision region [39]; however as the Airy wavefront moves towards later times the pulses reform and emerge having perturbed parameters. Since the truncated Airy pulse has the same center frequency and must maintain its first moment, it never completely crosses over the soliton; however the wavefront consisting of the main lobe, which has been designed to maintain its identity within the collision range, and subsequent lobes, do cross the soliton. (The Airy with our truncation coefficient of $a=0.005$ was designed to decay to half peak power at $\xi=16.7$, beyond the collision zone.) Therefore, the Airy-soliton interactions are classified as incomplete collisions, defined as having either an initial temporal overlap or a terminal overlap after the collision (occurring in our case), as opposed to complete collisions, (i.e. full crossing of the pulses achievable through non overlapping bandwidths and GVD [27,34,37]). These complete collisions, as present in wave division multiplexing (WDM) collisions, are known to be independent of relative phase and do not undergo a permanent frequency change after collision. Consequently, our findings show that the soliton undergoes a permanent frequency shift in some cases (Fig. 4.4 demonstrates the most extreme case for $\tau_0=-6$), and that the interaction (and frequency shift) is strongly dependent on relative phase, as in coherent soliton-soliton [23, 27] and soliton-CW [33] interactions.

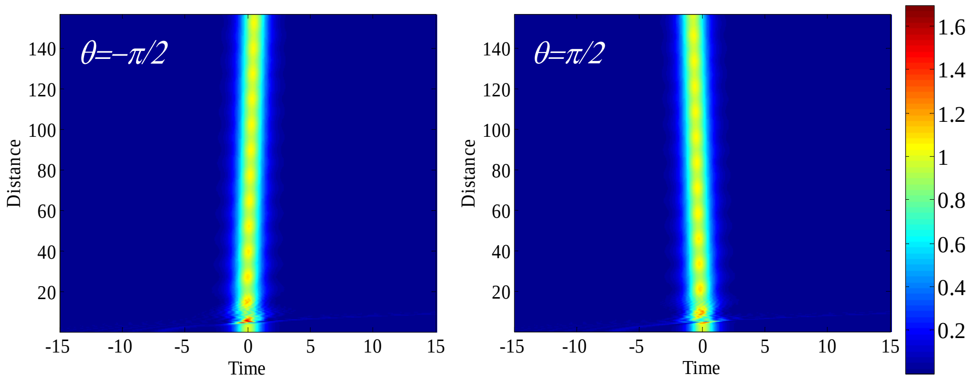

Fig. 4.4. Airy-soliton interaction with $\tau_0=-6$ and 8% intensity ratio showing a permanent frequency change when (a) $\theta=-\pi/2$, and (b) $\theta=\pi/2$ over $157\ L_D$ units (100 soliton periods).

An analysis of soliton-soliton collisions in WDM systems and coherent soliton interactions is carried in [27], offering an explanation for the dependence on relative phase or the lack of it based on perturbation theory developed by Haus *et. al*. [34, 35]. The derivation distinguishes between coherent and non-coherent interaction. For example, soliton-soliton collisions in a WDM system are regarded as incoherent interactions. The perturbation term taken into account in this case is only the cross phase modulation (XPM); the remaining terms originating from the NLSE nonlinear response are neglected due to rapid beating that average out to zero [39]. However, in the coherent derivation (i.e. soliton-soliton coherent interactions) the beat term between the two waveforms is taken into consideration.

Our investigative case bears similarity to coherent interactions at times, especially pronounced at closer initial separation while at other times the interaction is more incoherent in nature. A larger initial separation, the spectral repositioning by dispersion, results in an interaction between waveforms with a reduced spectral overlap. This distinction can be better understood by observing the Airy pulse evolution in time-frequency space as a function of propagation distance. Figure 5 shows the spectrogram (time-frequency space) of an evolving Airy pulse at different propagation distances (which basically shears the Airy spectrogram), demonstrating the spectral repositioning and the amount of spectral overlap of the colliding wavefront with the soliton. (The soliton's time-frequency signature is denoted by the green ellipse.) A more significant spectral overlap between soliton and Airy at point of collision is observed for an initial separation of $\tau_0=-6$ (compare middle column spectrograms in Fig. 4.5). Upon further propagation, the soliton propagates with quasi-CW light background from the dispersed Airy, demonstrated by the spectral overlap found in the right column in Fig. 4.5. As the propagation distance grows this dispersed background radiation becomes more monochromatic and approaches the same carrier frequency as the soliton. The continuous interaction results in oscillations of the solitons frequency and amplitude and therefore both the time position and phase will oscillate [33].

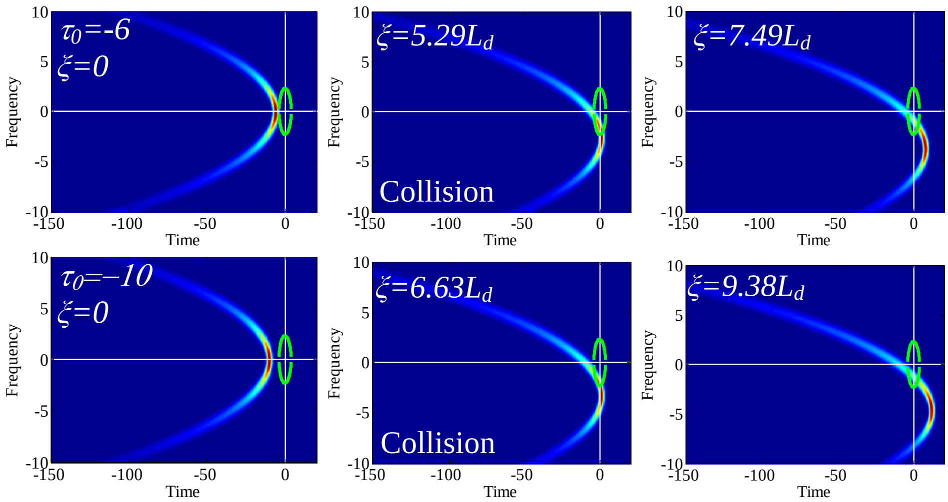

Fig. 4.5. Spectrogram of the Airy pulse at three selected distances for two initial separations; upper row: τ_0=*-6*, lower row: τ_0=*-10*. Left column: launch condition, center column: at collision distance (*5.29* L_D units and *6.63*, respectively), right column: at distance where Airy wavefront is at a temporal shift of twice the initial time separation (*7.49* L_D units and *9.38*, respectively). Green ellipse denotes the soliton extent over time and frequency.

4.2 Analysis

We track the soliton fundamental parameters prior to collision (ξ<3) and those of the perturbed emergent soliton (ξ>15) from the SSFM results, as we cannot extract any useful information throughout the collision region, as the soliton is indistinguishable.

We extract the emergent soliton characteristics from the numerical results and not resort to the well-developed perturbation theory analysis, as the Airy-soliton interaction case is incomplete [34]. Perturbation theory analysis requires the interaction to be complete and that the perturbation spectrum not exceeds that of the soliton, neither of which holds for the Airy pulse [34]. Furthermore, the perturbation theory analysis is intensity based, eliminating the relative phase dependence of the pulses, which is present in our Airy-soliton interaction. (Although, it may be possible to expand the perturbation theory to encompass this scenario as well, see appendix A).

To derive high resolution emergent soliton parameters devoid of sampling effects, we locate the intensity peak at each propagation distance, select a sufficient number of intensity samples around the peak value, and then apply a sech(•)^2 intensity profile fit to the selected samples. The benefit of this procedure is that it allows us to construct a continuous soliton intensity profile with respect to time at a given distance, from which we extract the intensity, time position, and temporal width at high resolution and with no discretization effects. This procedure generates smoothly varying curves for the soliton parameters' evolution. (The soliton phase is extracted from the sample with peak intensity.)

4.2.1 Soliton power

The soliton peak power behavior is analyzed along the propagation range and is charted in Fig. 4.6a for the closest Airy-soliton separation (τ_0=-6), highest Airy power (*8%*) and for two representative relative phases (*0 , π*). The emergent soliton exhibits peak power oscillations that are dependent on the colliding Airy pulse phase. We further see that the two curves are vertically displaced, indicating a different mean soliton intensity (both oscillate nearly about the launched (original) soliton peak power). We next chart the mean peak soliton intensity for different initial Airy phases and launched powers at $\tau_0=-6$ (see Fig 4.6-b). (The mean soliton intensity is calculated far from collision, by establishing soliton power and background power from the maximum and minimum interference values. These interferences are due to the soliton's natural SPM.) We observe sinusoidal dependence on the initial Airy phase for all powers, indicating an energy transfer between the pulses during the primary collision [19]. Similar sinusoidal behavior is observed at larger time separations (i.e., $\tau_0=-8$ and $\tau_0=-10$), albeit at a lesser magnitude (Fig. 4.6-c shows mean intensity fluctuation only at the *8%* collision intensity for clarity). Since the overall colliding energy is the same, regardless of initial time separation (i.e., all energy contained in the Airy's delayed lower frequency components), the less pronounced effect at larger initial separations demonstrates that with greater time separation a more incoherent collision between soliton and the Airy occurs due to a larger frequency offset at collision (as previously explained by spectrograms). For the largest time separation we find that the mean intensity is nearly unchanged, while for the shortest time separation the mean intensity is predominantly linearly dependent on Airy amplitude, indicating coherent interaction behavior (Fig. 4.6-d).

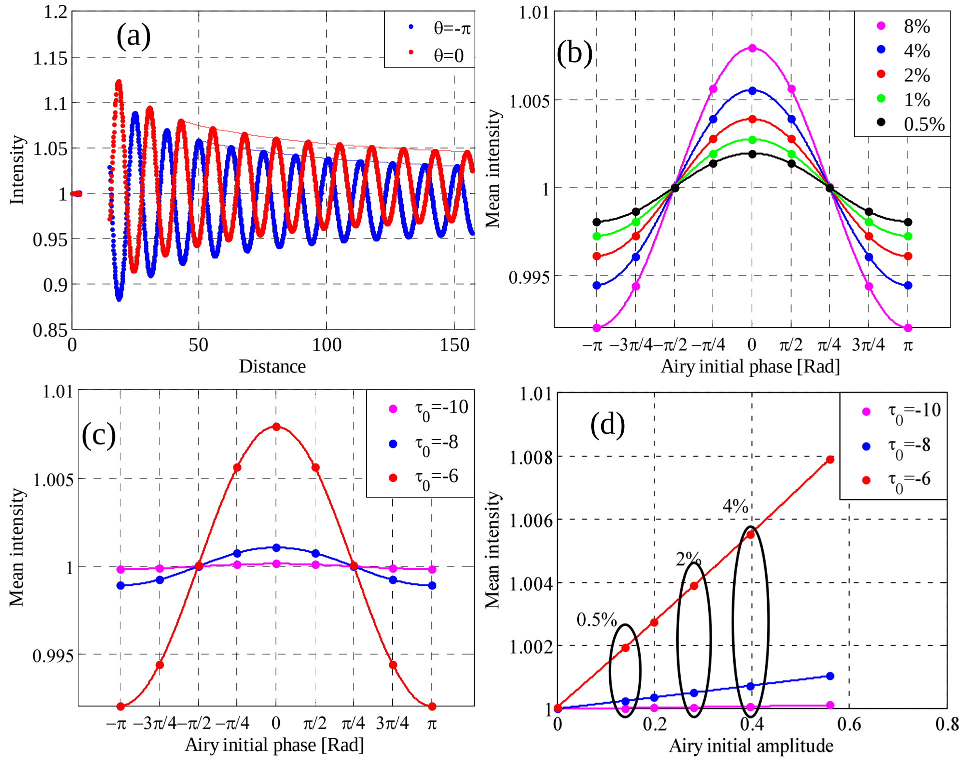

Fig. 4.6. Soliton intensity oscillations. (a) Intensity oscillation (intensity ratio of 8% and τ_0=-6). Also shown envelope fit of the form $1/\sqrt{z}$, (b) Mean intensity of the oscillations with a sinusoidal fit, (c) dependence with respect to the Airy's initial phase for all the time separations (intensity ratio of 8%), (d) Mean intensity for all separations with at *8%* intensity ratio for the $\theta=0$, (with a second order polynomial fit; behavior predominantly linear) .

We also see the intensity oscillations decay in magnitude along the propagation as the soliton relaxes. The functional form of the decay is in agreement with [39, 40, 41] that states that within the region of the asymptotic solution the non-soliton part decays as $\xi^{-1/2}$ (Fig. 4.6-a). The period between oscillations varies slightly from one oscillation to another (on account of the dispersed Airy background center frequency approaching that of the soliton), converging towards a constant period of 4π distance units (corresponding to the distance a soliton accumulates 2π phase), as the soliton propagates away from the collision region. The beating comes from the interference between the soliton SPM with the dispersed, now quasi-CW, Airy background.

4.2.2 Soliton Time and Center Frequency

We next track the soliton change in time position (e.g. Fig. 3, $\theta=-\pi$). Solitons experience time position change through local frequency changes during the collision and permanent frequency changes which map to time position alterations by group velocity dispersion (GVD) [33,35-38]. Fig. 4.7 plots the soliton time shift for several phases at collision with *8%* Airy pulses for each of the three investigated time separations (τ_0=–6, –8, –10). The most prominent feature is a soliton permanent frequency change after the main collision, which occurs after the collision with the Airy's wavefront and is much more pronounced at closer initial time separations. The frequency change is also strongly dependent on relative phase between the Airy and soliton, and can be positive or negative (soliton travels slower or faster, respectively). As the propagation progresses, the time shift oscillates about the time shift induced solely by the permanent frequency change. These oscillations are attributed to the ongoing propagation through the dispersed Airy and are dependent on its amplitude and frequency detuning [33]. All solitons also experience a discrete time shift after the primary collision, which appears weakly dependent on the initial time separation and phase.

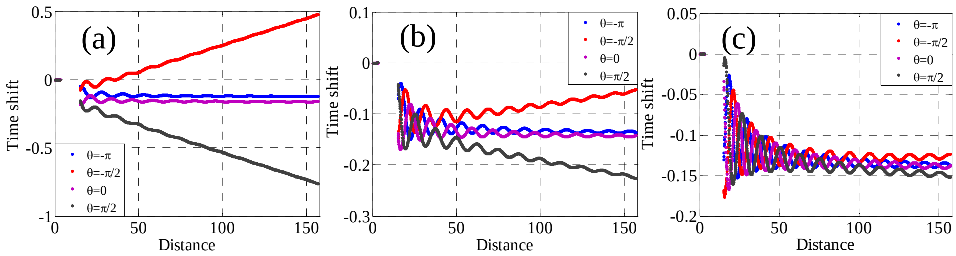

Fig. 4.7. Time shift for all initial separations with an 8% intensity ratio for selected phases.
(a) τ_0=–6, (b) τ_0=–8 , (c) t_0=-10. Note that the scale of the time shift is not identical in all three cases.

We find the permanent frequency change experienced by the soliton by applying a linear fit to each trace in Fig. 4.7 (the fit is performed from about mid propagation distance up the end), where the slope represents the frequency change. The frequency change is dramatically stronger for closer time separations (Fig. 4.8-a, for $\theta=-\pi/2$ at which a large positive frequency change is observed for all separations), while for larger separations the frequency change eventually disappears. This behavior is in line with our previous finding that at small initial separations the collision has coherent interaction characteristics, while for larger separations the collision is incoherent (exhibiting no permanent frequency change). This conclusion is supported by the linear dependence on Airy amplitude for the closest time separation (τ_0=–6). The permanent frequency change is also sinusoidally dependent on the Airy phase (Fig. 4.8-b).

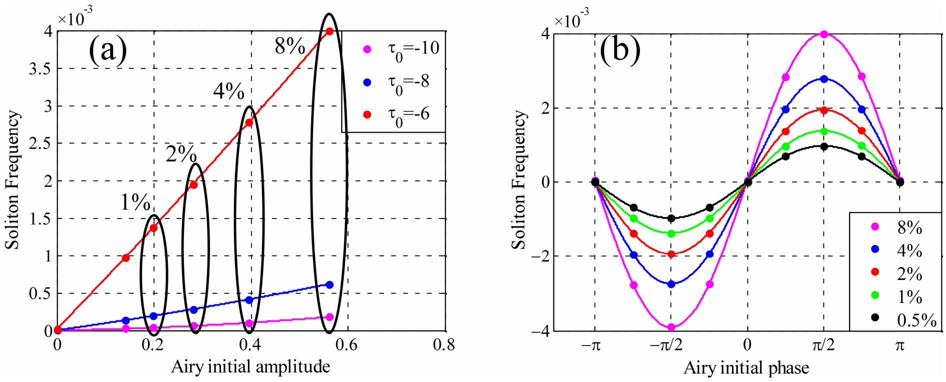

Fig. 4.8. (a) Soliton frequency change with respect to amplitude at $\theta=\pi/2$, (b) Sinusoidal fit with respect to Airy phase for all amplitudes with $\tau_0=-6$ of the frequency change.

We plot the soliton discrete time shifts after the primary collision for all separations at different Airy intensities and its weak phase dependence in Fig. 4.9. The time shifts are all negative (towards the Airy wavefront) as in complete collisions [27, 34, 38], depend quadratically on the Airy's initial amplitude with little dependence on initial separation (Fig. 4.8-a), and are hardly dependent on Airy initial phase (Fig. 4.8-b). This behavior bears the signature of complete collisions with the main and subsequent lobes [34, 27]. To obtain an estimate for the discrete time shift generated by the primary collision (which is within the collision zone, hence masked by interference), we use the linear fit lines for the soliton time position (previously used to measure the frequency change) calculated at the collision distances given by Eq. (4.4) for each initial time separation case. Hence, the primary collision results in a nearly fixed discrete time shift for the soliton and bears the signature of complete collision, while the soliton acquires a permanent frequency change during the same collision for close Airy launch (coherent collision characteristic, due to the spectral overlap at collision).

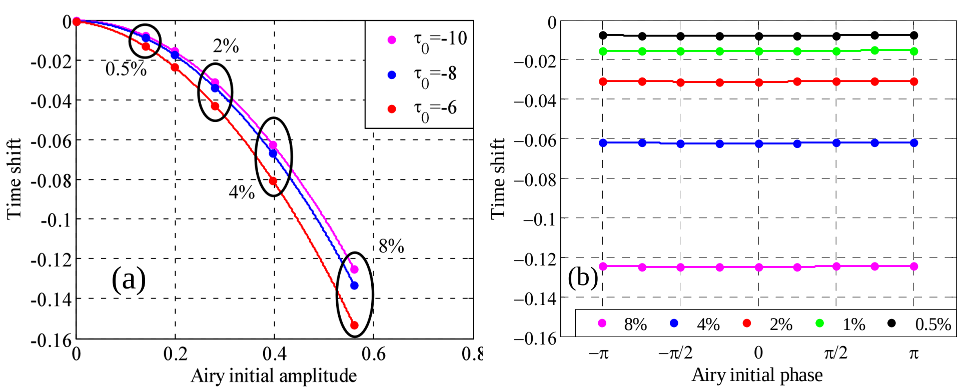

Fig. 4.9. Estimated time shift form, (a) Time shift with respect to Airy's initial amplitude for all initial time separations ($\theta=0$), Time shift with respect to Airy's initial phase and amplitude with $\tau_0=-10$ and a sinusoidal fit profile .

4.2.3 Soliton Phase

The last emergent soliton parameter we follow is the phase. Solitons continuously acquire phase along the propagation distance, and we subtract this constant term in all our results (using the launched soliton parameters) so that we only witness the phase difference between that of the expected phase of the unperturbed soliton and that of emergent soliton (see Fig. 4.10 for 8% Airy intensity for all the separations and select phases). As in the time shift results (Fig. 4.6), we see a discrete phase offset after the primary collision, in all cases equaling about 0.2 radians, and divergent and oscillatory phase in the relaxation region. While the oscillatory behavior is explained by the continuous interaction with the dispersed Airy background radiation (resultant of local intensity and frequency oscillations), the linear component is a reflection of the emergent soliton perturbed parameters of mean intensity and center frequency. Both terms contribute to the accumulated phase linearly with respect to ξ and quadratically on the amplitude and frequency changes of the soliton [27]. For example, in Fig. 4.10-a we see that for the initial phases of $\theta=-\pi$ and $\theta=0$ there is a linearly-dependent phase difference attributed solely to a change in mean intensity, as the emergent soliton had only a mean intensity change (see Fig. 4.6-b) and no permanent frequency change (see Fig. 4.8-b) for these launched conditions. (A change of approximately 0.4 radian is accumulated between distances of 50 to 150, which translates to mean intensity change of approximately 0.008, exactly as found in Fig. 4.6-b). In addition, we find that for the case of $\theta=-\pi/2$ and $\theta=\pi/2$ the small change in frequency of approximately 4×10^{-3} results in a negligible change since the phase term is quadratically dependent on frequency change.

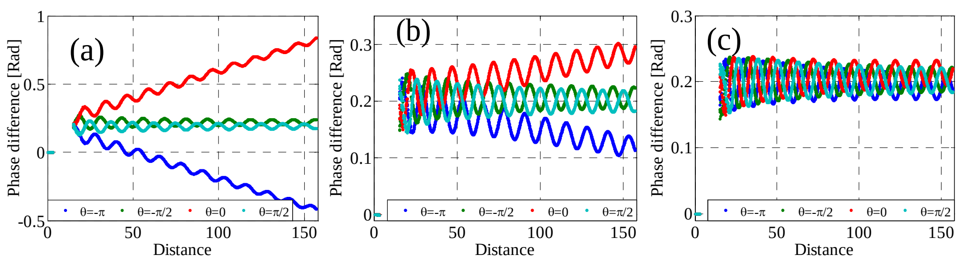

Fig. 4.10. Phase difference along the Airy propagation for select Airy initial phases with an intensity ratio of *8%* (a) $\tau_0=-6$, (b) $\tau_0=-8$, (c) $\tau_0=-10$.

5 Conclusions

We have demonstrated the unique attributes of the interaction between a colliding Airy pulse and a soliton pulse at the same center frequency through split-step Fourier method simulations. The interactions are made possible by the ballistic trajectory property of the Airy pulse.

Our findings show that the interactions are described by two regions of propagation. The first region, at which the primary collision occurs with the intense main lobe of the Airy wavefront, it is responsible for the main change of the soliton fundamental parameters. The nature of the interaction at the primary collision is strongly dependent on the initial Airy-soliton time separation, varying from coherent to incoherent interaction. At close separations, the collision event is accompanied by spectral overlap between the Airy and soliton. This results in a coherent interaction that perturbs the soliton frequency and amplitude. At larger initial time separations, the interaction is incoherent as there is a decrease in spectral overlap and the rapidly oscillating phase of the interference term does not accumulate to significant frequency and amplitude changes. In both cases, however, the soliton does experience a discrete time and phase change, due to a complete collision with the Airy main lobe. The second region of propagation is beyond the collision event, which is primarily defined by continuous interactions with the dispersed Airy tail, resulting in oscillations of the time shift and phase through local intensity and amplitude changes respectively. The soliton experience slow relaxation throughout this secondary region, as the Airy disperses and the oscillations’ magnitude diminishes.

The nature of the interactions that were simulated are of collisions. In all cases, the Airy pulse propagated through the soliton pulse. This is in contrast to an intense soliton acting as an event horizon that can block the Airy pulse propagation [45]. An interesting future research effort could be to investigate the conditions leading to a soliton barrier, by possibly choosing a more intense and shorter duration soliton. In our simulations the Airy bandwidth exceeds that of the soliton, emphasizing the effect of dispersion.

While we performed all our analysis in one dimensional temporal media, i.e. dispersive and nonlinear fiber propagation, all our findings should hold in one and two dimensional spatial propagation cases in Kerr media as the underlying equations defining the interactions are isomorphic.

References:

1. J. Durnin, “Exact solutions for nondiffracting beams. I. The scalar theory,” J. Opt. Soc. Am. A **4**, 651-654 (1987).
2. J. Durnin, J. J. Miceli Jr., and J. H. Eberly, “Diffraction-free beams,” Phys. Rev. Lett. **58,** 1499-1501 (1987).
3. M. V. Berry and N. L. Balazs, “Nonspreading wave packets,” Am. J. Phys. **47**, 264-267 (1979).
4. G. A. Siviloglou and D. N. Christodoulides, “Accelerating finite energy Airy beams,” Opt. Lett. **32**, 979-981 (2007).
5. G. A. Siviloglou, J. Broky, A. Dogariu and D. N. Christodoulides, “Observation of Accelerating Airy Beams,” Phys. Rev. Lett. **99**, 213901 (2007).
6. G. A. Siviloglou, J. Broky, A. Dogariu and D. N. Christodoulides, “Ballistic dynamics of Airy beams,” Opt. Lett. **33**, 207-209 (2008).
7. P. Polynkin, M. Kolesik, J. V. Moloney, G. A. Siviloglou and D. N. Christodoulides, “Curved Plasma Channel Generation Using Ultraintense Airy Beams,” Science **324**, 229-232 (2009)
8. J. Baumgartl, M. Mazilu and K. Dholakia, “Optically mediated particle clearing using Airy wavepackets,” Nat. Photon. **2**,675-678 (2008).
9. A. Salandrino and D. N. Christodoulides, “Airy plasmon: a nondiffracting surface wave,” Opt. Lett. **33**, 2082-84 (2010).
10. J. Broky, G. A. Siviloglou, A. Dogariu, and D. N. Christodoulides, “Self-healing properties of optical Airy beams,” Opt. Express **16**, 12880-91 (2008).
11. F. O. Fahrbach, P. Simon, and A. Rohrbach, “Microscopy with self-reconstructing beams,” Nat. Photon.
12. A. Chong, W. H. Renninger, D. N. Christodoulides and F. W. Wise, “Airy-Bessel wave packets as versatile linear light bullets,” Nat. Photon. **4**, 103-106 (2010).
13. G. P. Agrawal and M. J. Potasek, “Nonlinear pulse distortion in single-mode optical fibers at the zero-dispersion wavelength,” Phys. Rev. A **33**, 1765-1776 (1986).
14. D. Abdollahpour, S. Suntsov, D. G. Papazoglou, S. Tzortzakis, “Spatiotemporal Airy light bullets in the linear and nonlinear regimes,” Phys. Rev. Lett. **105**, 253901 (2010).
15. D. G. Papazoglou, N. K. Efremidis, D. N. Christodoulides, and S. Tzortzakis, “Observation of abruptly autofocusing waves,” Opt. Lett. **35**, 1842-4 (2011).
16. R.-P. Chen, C.-F. Yin, X.-X. Chu, and H. Wang, “Effect of Kerr nonlinearity on an Airy beam,” Phys. Rev. A **82**, 043832 (2010).
17. I. Kaminer, M. Segev, D.N. Christodoulides, “Self-Accelerating Self-Trapped Optical Beams,” Phys. Rev. Lett. **106**, 213903 (2011).
18. Y. Fattal, A. Rudnick, D. M. Marom, “Soliton shedding from Airy pulses in Kerr media,” Opt. Express 19, 17298-307 (2011).
19. I. Dolev, T. Ellenbogen and A. Arie, “Switching the acceleration direction of Airy beams by a nonlinear optical process,” Opt. Lett. **35,** 1581-1583 (2010).
20. A. Bahabad, M. M. Murnane, H. C. Kapteyn, “Manipulating nonlinear optical processes with accepterating light beams,” Phys. Rev. A **84**, 033819 (2011).
21. V. E. Zakharov and A. B. Shabat, “Exact Theory Of Two-Dimensional Self-Focusing and One-Dimensional Self-Modulation Of Waves in Nonlinear media,” Sov. Phys. JETP **34**, 62-69 (1972).
22. A. Hasegawa and F. Tappert, “Transmission of stationary nonlinear optical pulses in dispersive dielectric fibers. I. Anomalous dispersion,” Appl. Phys. Lett. 23, 142-4 (1973).
23. G. P. Agrawal, *Nonlinear Fiber Optics*, 3rd ed. (Academic Press, Boston, 2001)
24. G.I. Stegeman and M. Segev, “Optical Spatial and Their Interactions: Universality and Diversity,” Science **286**, 1518-23 (1999).
25. J. R. Taylor, *Optical Solitons Theory and Experiment* (Cambridge, U.K.: Cambridge Univ. Press, 1992).
26. H. A. Haus and W. S. Wong, “Solitons in optical communications,” Rev. Mod. Phys. **68**, 423-444 (1996).
27. E. Iannone, F. Matera, A Mecozzi and M. Settembre, *Nonlinear Optical Communication Networks* (Wiley, New York, 1998).
28. A.Hasegawa “Numerical study of optical soliton transmission amplified periodically by the stimulated Raman process”, Appl. Opt. **23**, 3302-3309,(1984).

29. L.F. Mollenauer, R.H. Stolen and J.P. Gordon, "Experminatl observation of picosecond pulse narrowing and solitons in optical fibers",Phys. Rev. Lett. **45**,1095-1098,(1980).
30. G. P. Gordon, "Interaction forces among solitons in optical fibers," Opt. Lett. **8**, 596-598 (1983).
31. F. M. Mitschke and L.F Mollenauer, "Experimental observation of interactions forces between solitons in optical fibers," Opt. Lett. **12**, 355-357 (1987).
32. L. F. Mollenauer, S. G. Evangelides and J. P. Gordon, "Wavelength Division Multiplexing with Solitons in Ultra-Long Distance Transmission Using Lumped Amplifiers," J. Lightwave Technol. **9**, 362-367 (1991).
33. A. Hasegawa and Y. Kodama, "Amplification and reshaping of optical solitons in a glass-fiber—I," Opt. Lett. **7**, 285-287 (1982).
34. H. A. Haus, F. I. Khatri, W. S. Wong, E. P. Ippen and K. R. Tamura, "Interaction of Solitons with Sinusoidal Wave Packet," IEEE J. Quantum Electron. **32**, 917-924 (1996).
35. H. A. Haus, W. S. Wong, and F. I. Khatri, "Continuum generation by perturbation of Soliton," J. Opt. Soc. Am. B **14**, 304-313 (1997).
36. Q. H. Park and H. J. Shin, "Parametric Control of Soliton Light Traffic by cw Traffic Light," Phys. Rev. Lett. **82**, 4432-4435 (1999).
37. H.J. Shin, "Soliton scattering from a finite cnoidal wave train in a fiber," Phys. Rev. Lett. E. **63**, 026606 (2001).
38. H.J. Shin, "Interaction of a soliton with a continuous wave packet," Phys. Rev. Lett. E. **67**, 017602 (2003).
39. E. A. Kuznetsov, A. V. Mikhailov and I. A. Shimokhin, "Nonlinear interaction of solitons and radiation," Physica D 87, 201-205 (1995).
40. E. A Kuznetson and A. V Mikhailov, "Relaxation oscillations of solitons," Pisma Zh. Eksp. Teor. Fiz. **60**, 466-470 (1994).
41. J. Satsuma and N. Yajima, "Initial Value Problems of One-Dimensional Self-Modulation of Nonlinear Waves in Dispersive Media," Suppl. Prog. Theo. Phys. No. **55** (1974).
42. R.Boyd., *Nonlinear Optics*, 3rd ed. (Academic Press, Boston, 2008)
43. B.E.A. Saleh and M.C. Teich, *FUNDAMENTALS OF PHOTONICS*,2nd (John Wiley &Sons,Inc,Hoboken,New Jersey).
44. Wolfram http://functions.wolfram.com/Bessel-TypeFunctions/AiryAi/
45. T. G. Philbin, C. Kuklewicz, S. Robertson, S. Hill, F. König, and U. Leonhardt, "Fiber-Optical Analog of the Event Horizon," Science 319, 1367-1370 (2008).
46. C. Yeh and L. Bergman, "Pulse shepherding in nonlinear fiber optics," J. Appl. Phys. 80, 3174-78 (1996).

6 Appendix

6.1 *The Perturbation theory:*

In this section we will briefly review the fundamentals of the perturbation theory developed by Haus *et. al.* and discusses in brief the modifications needed to expand the perturbation found in ref. [34] to encompass out scenario as well. In ref. 34 the interactions are of the incoherent type and are only intensity dependent. Since the Airy-soliton perturbation is quasi- coherent it is necessary to also review coherent interactions as well.

6.1.1 Theory

Let us first define the dimensionless NLSE; we begin by defining these dimensionless variables.

$$\tau = \frac{T}{T_0}; \quad \xi = \frac{z}{L_D} \quad U = \frac{A}{\sqrt{P_0}} \tag{6.1}$$

To further simplify we also define: $u = \sqrt{\gamma L_D} A$ and Eq. (2.21) transforms it to Eq. (6.2) which is the dimensionless form of the NLSE.

$$\frac{\partial u}{\partial \tau} = \frac{i}{2}\frac{\partial^2 u}{\partial \tau^2} + i|u|^2 u \tag{6.2}$$

In Eq. (2.43) we assume that $\mathrm{sgn}(\beta_2) = -1$, which is the appropriate choice from anomalous media. For Eq. (6.2) the fundamental soliton presentation is [27]:

$$u_0(\tau,\xi) = A\,\mathrm{sech}\left(A\left(\tau - \tau_0 - \Omega\xi\right)\right)\exp\left(-i\Omega\tau + \frac{i}{2}\left(A^2 - \Omega^2\right)\xi + i\phi_0\right) \tag{6.3}$$

τ- the dimensionless time.
Ω-the dimensionless center frequency.
A-amplitude.

To generalize Eq. (6.2) we shall add a perturbation term to the equation [27].

$$\frac{\partial u}{\partial \xi} = \frac{i}{2}\frac{\partial^2 u}{\partial \tau^2} + i|u|^2 u + R \tag{6.4}$$

The perturbation term *R*, can be a function of τ,ξ and of u_0, u_0* and any of their derivatives. We proceed under the assumption that the terms found in R are small so that its influence on the soliton dynamics can be treated to first order.

Consider the case $\Omega = 0$ and assume a solution of the form:

$$u(\tau,\xi) = u_0(\tau,\xi) + \delta(\tau,\xi)\exp\left(\frac{i}{2}A^2\xi\right) \tag{6.5}$$

Equation (6.5) is composed of the fundamental soliton along with a small perturbation from it. The perturbation term is a multiplication of two terms, the perturbation ($\delta(\tau,\xi)$) and its SPM. Substitution of Eq. (6.5) in to Eq. (6.4) is the first step for the basis of the soliton perturbation theory. Since the detailed mathematical derivation is complex and lengthy it will not be developed here [27]. However, the basis of the theory along with its application will be demonstrated in short. Returning to the substitution we arrive at:

$$\delta u = \frac{\partial u_0}{\partial A}\delta A + \frac{\partial u_0}{\partial \phi}\delta\phi + \frac{\partial u_0}{\partial \Omega}\delta\Omega + \frac{\partial u_0}{\partial \tau_0}\delta\tau_0 + \delta u_c\left(\tau,\zeta\right) \tag{6.6}$$

The latter equation can be interpreted as two distinct contributions from the perturbation. The first is composed of all the terms having derivatives of u_0 and the second is that labeled δu_c. They physical meaning of this is: The first is responsible for any displacements of the soliton parameters while the second is any change to the field that cannot be reduced to changes in the soliton parameters, an excitation of the so called soliton "continuum". The above derivatives found in Eq. (6.6) can be expressed with the linear combination of these four base functions.

$$f_A = \frac{1}{A}\left\{1 - A\left(\tau-\tau_0\right)\tanh\left(A\left(\tau-\tau_0\right)\right)\right\}u_0 \tag{6.7}$$

$$f_\phi = iu_0 \tag{6.8}$$

$$f_\Omega = -i\left(\tau-\tau_0\right)u_0 \tag{6.9}$$

$$f_{\tau_0} = A\tanh\left(A\left(\tau-\tau_0\right)\right)u_0 \tag{6.10}$$

Correlating (Eq. (6.7)-(6.10)) these definitions to the derivatives in Eq. (6.6) we get Eq.(6.11). The weight (amplitude) of each change is the factor found after each base function in Eq.(6.11). To find the magnitude of the change for each soliton parameter it is necessary to define the inner product for this function space Eq.(6.12). The physical meanings of the terms found in Eq.(6.11) are the displacements of the j[th] soliton parameter by $f_j\Delta j$ with f_j properly taking care to modify the j[th] parameter only of the soliton.

$$\delta u = f_A\delta A\left(\xi\right) + f_\phi\delta\phi\left(\xi\right) + f_\Omega\delta\Omega\left(\xi\right) + f_{\tau_0}\delta\tau_0\left(\xi\right) + \delta u_c\left(\tau,\zeta\right) \tag{6.11}$$

$$\left\langle f \,|\, g\right\rangle = \mathrm{Re}\int d\tau\, f^* g \tag{6.12}$$

To attain the proper factor for each term it is necessary to project the perturbation on the adjoint space with the aid of the inner product previously defined. This now requires us to define the adjoint base functions:

$$\underline{f}_A = -i f_\phi \tag{6.13}$$

$$\underline{f}_\phi = i f_A \tag{6.14}$$

$$\underline{f}_\Omega = -\frac{i}{A} f_{\tau_0} \tag{6.15}$$

$$\underline{f}_{\tau_0} = \frac{i}{A} f_\Omega \tag{6.16}$$

At this stage, it is important to note here that the soliton continuum is perpendicular to these functions and therefore as stated previously does not contribute to these values. Therefore, we can continue with the projection of the perturbation on the adjoint functions.

$$\frac{d\delta A}{d\xi} = \mathrm{Re}\int d\tau\, \underline{f}_A^* R \tag{6.17}$$

$$\frac{d\delta\phi}{d\xi} = A\delta A + \tau_0 \frac{d\delta\Omega(\xi)}{d\xi} + \mathrm{Re}\int d\tau\, \underline{f}_\phi^* R \tag{6.18}$$

$$\frac{d\delta\Omega}{d\xi} = \mathrm{Re}\int d\tau\, \underline{f}_\Omega^* R \tag{6.19}$$

$$\frac{d\delta\tau_0}{d\xi} = -\delta\Omega + \mathrm{Re}\int d\tau\, \underline{f}_{\tau_0}^* R \tag{6.20}$$

The first equation in this set of four governs the variations in amplitude of the soliton as it undergoes the perturbation. The second governs the phase profile at each distance. The additional terms found in the phase derivative (Eq. (6.18)) (other than the projection term) are brought about by dependence of the exponential phase term in (Eq.(6.3)) on both frequency and amplitude (the dependence on amplitude is the SPM) which is reflected in Eq.(6.18). The third and fourth are the variations in center frequency and the first momentum in time (time position-τ_0) respectively. As seen in Eq. (6.20) there are two contributions, the first is the projection and the second is the contribution from frequency variations. Which is apparent in the translations in time as indicated by the $\Omega\xi$ in the $\mathrm{sech}(\bullet)$ argument (Eq.(6.3)) .The above equations are correct when the changes in the observables are small. Though, it is possible to expand these equations to further accommodate large change in the observables but this is beyond the scope of derivation.

6.1.2 Incoherent soliton interactions

In ref. [34] and [27] the interactions are of the incoherent type between two solitons (Eq.(6.21)) of different wavelengths (and not between solitons as successive bits) in a wavelength division multiplexing (WDM) systems. To insure an incoherent interaction the condition $\left|\Omega_1 - \Omega_2\right| \gg 1$ must be satisfied.

$$u(\tau,\xi) = u_1(\tau,\xi) + u_2(\tau,\xi) \tag{6.21}$$

Where $u_j(\tau,\xi)$ is:

$$u_j(\tau,\xi) = A_j \operatorname{sech}\left(A_j\left(\tau - \tau_{0j}(\xi)\right)\right)\exp\left(-i\Omega_j(\xi) + i\phi_j(\xi)\right) \tag{6.22}$$

Rewriting Eq. (6.4) for *u1* after substitution of(6.21):

$$\frac{\partial u_1}{\partial \tau} = \frac{i}{2}\frac{\partial^2 u_1}{\partial \tau^2} + i\left|u_1 + u_2\right|^2 u_1 \tag{6.23}$$

Under the condition imposed on the frequency separation, it is possible to neglect the terms oscillating at the frequency $\Omega_1 - \Omega_2$. Therefore, Eq. (6.23) can be approximated by:

$$\frac{\partial u_1}{\partial \tau} = \frac{i}{2}\frac{\partial^2 u_1}{\partial \tau^2} + i\left|u_1\right|^2 u_1 + \underbrace{2i\left|u_2\right|^2 u_1}_{XPM} \tag{6.24}$$

From here we can recognize the perturbation term R as the XPM:

$$R = 2i\left|u_2\right|^2 u_1 \tag{6.25}$$

In this case we can clearly see that interaction is not influenced by the field of the perturbation but on its intensity distribution which is the same as in [34]. Therefore, to expand on the perturbation theory we need to take a look at coherent interactions.

6.1.3 Coherent soliton interactions

An example of a coherent interaction [27] is between two solitons at the same center frequency with a certain time separation $\left(\left|T_1 - T_2\right| \gg \max(1/A_1, 1/A_2)\right)$ that are launched into to the fiber (successive bits in a stream). During propagation they interact through the tail end of one another.

Substituting equation (6.21) in to (6.4) the nonlinear term will produce the following:

$$i\left|u_1 + u_2\right|\left(u_1 + u_2\right) : \; i\left|u_1\right|^2 u_1 + 2i\left|u_1\right|^2 u_2 + iu_1^2 u_2^* \tag{6.26}$$

Since the dominate terms arises' from the tail of soliton 2 on soliton 1 (and vice versa) when $\tau \approx T_1$, the terms retained from Eq. (6.26) are those of SPM and first-order terms in u_2. From here we can also define the perturbation term *R* in(6.4).

$$R = 2i\left|u_1\right|^2 u_2 + iu_1^2 u_2^* \tag{6.27}$$

Equation (6.27) shows that interaction is dependent on the field of the tail of soliton 2 that is in the vicinity of soliton 1 and thus is phase dependent. It also shows that the intensity and amplitudes have influence on the interaction.

6.1.4 Airy-soliton expansion

From this point we can expand the perturbation to encompass the Airy perturbation of a soliton by using Eq. (6.27) as the perturbation term in equations (6.17)-(6.20). However, substitution of Eq. (4.2) as u_1 and Eq. (4.1) as u_2 we will have to solve the evolution integrals for the soliton parameters numerically. This so, since the Airy function does not have an indefinite integral. Resulting in a process similar to that of the SSFM, but allows for following the soliton parameters during the collision process as well.

7 Submitted papers

Airy-Soliton Interactions in Kerr Media*

Amitay Rudnick and Dan M. Marom*

Department of Applied Physics, Hebrew University of Jerusalem, Jerusalem, 91904, Israel
*danmarom@cc.huji.ac.il**

Abstract: We investigate and analyze temporal soliton interactions with a dispersive truncated Airy pulse traveling in a nonlinear fiber at the same center wavelength (or frequency), via split step Fourier numerical simulation. Truncated Airy pulses, which remain self-similar during propagation and have a ballistic trajectory in the retarded time frame, can interact with a nearby soliton by its accelerating wavefront property. We find by tracking the fundamental parameters of the emergent soliton—time position, amplitude, phase and frequency—that they alter due to the primary collision with the Airy main lobe and the continuous co-propagation with the dispersed Airy background. These interactions are found to resemble coherent interactions when the initial time separation is small and incoherent at others. This is due to spectral content repositioning within the Airy pulse, changing the nature of interaction from coherent to incoherent. Following the collision, the soliton intensity oscillates as it relaxes. The initial parameters of the Airy pulse such as initial phase, amplitude and time position are varied to better understand the nature of the interactions.

OCIS codes: (190.0190) Nonlinear optics; (190.3270) Kerr effect; (060.5530) Pulse propagation and temporal solitons

Received 14 Jul 2011; revised 3 Nov 2011; accepted 13 Nov 2011; published 30 Nov 2011

(C) 2011 OSA 5 December 2011 / Vol. 19, No. 25 / OPTICS EXPRESS 25570

---

*Chapter 4 follows this paper

Soliton shedding from Airy pulses in Kerr media

Yiska Fattal, Amitay Rudnick and Dan M. Marom

Department of applied physics, Hebrew University, Givat Ram, Jerusalem 91904, Israel
[*]yiska.fatal@mail.huji.ac.il

Abstract: We simulate and analyze the propagation of truncated temporal Airy pulses in a single mode fiber in the presence of self-phase modulation and anomalous dispersion as a function of the launched Airy power and truncation coefficient. Soliton pulse shedding is observed, where the emergent soliton parameters depend on the launched Airy pulse characteristics. The Soliton temporal position shifts to earlier times with higher launched powers due to an earlier shedding event and with greater energy in the Airy tail due to collisions with the accelerating lobes. In spite of the Airy energy loss to the shed Soliton, the Airy pulse continues to exhibit the unique property of acceleration in time and the main lobe recovers from the energy loss (healing property of Airy waveforms).

OCIS codes: (190.0190) Nonlinear optics; (190.3270) Kerr effect; (060.5530) Pulse propagation and temporal solitons.

References

47. M. V. Berry and N. L. Balazs, "Nonspreading Wave Packets," Am. J. Phys. 47, 264-267 (1979)
48. G. A. Siviloglou, J. Broky, A. Dogariu, and D. N. Christodoulides, "Ballistic dynamics of Airy beams," Optics Letters **33**(3), 207-209 (2008).
49. Jörg Baumgartl, Michael Mazilu and Kishan Dholakia, "Optically mediated particle clearing using Airy wavepackets," Nature Photonics **2**, 675 - 678 (2008).
50. Ido Dolev, Tal Ellenbogen, and Ady Arie, "Switching the acceleration direction of Airy beams by a nonlinear optical process," Optics Letters **35**, 1581-1583 (2010)
51. Pavel Polynkin1, Miroslav Kolesik, Jerome V. Moloney, Georgios A. Siviloglou and Demetrios N. Christodoulides, " Curved Plasma Channel Generation Using Ultraintense Airy Beams," Science **10**, 194-195 (2009).
52. Pavel Polynkin, Miroslav Kolesik, and Jerome Moloney, "Filamentation of Femtosecond Laser Airy Beams in Water," Phys. Rev. Lett. **103**, 123902-123905 (2009)
53. Andy Chong, William H. Renninger, Demetrios N. Christodoulides and Frank W. Wise, "Airy–Bessel wave packets as versatile linear light bullets," Nature Photonics **4**, 103 - 106 (2010).
54. Daryoush Abdollahpour, Sergiy Suntsov, Dimitrios G. Papazoglou, and Stelios Tzortzakis, "Spatiotemporal Airy Light Bullets in the Linear and Nonlinear Regimes," Phys. Rev. Lett. **105**, 253901-253904 (2010).
55. C. Ament, P. Polynkin, and J. V. Moloney, "Supercontinuum Generation with Self-Healing Airy Pulses," in CLEO:2011 - Laser Applications to Photonic Applications, OSA Technical Digest (CD) (Optical Society of America, 2011), paper PDPC9.
56. Rui-Pin Chen, Chau-Fu Yin, Xiu-Xiang Chu, Hui Wang, "Effect of Kerr Nonlinearity on an Airy Beam," Phys. Rev. A **82,** 043832-043835, (2010).
57. John Broky, Georgios A. Siviloglou, Aristide Dogariu, and Demetrios N. Christodoulides, "Self-healing properties of optical Airy beams," Optics Express **16**(17) ,12880-12891 (2008).
58. N. Belanger and P. A. Belanger, "Bright solitons on a cw background," Optics Communications **124**, 301-308 (1996).
59. Michel W Chbat, Paul R. Prucnal, Mohammed N. Islam, Carl E. Soccolich, and James P. Gordon, "Long-range interference effects of soliton reshaping in optical fibers," JOSA B **10**(8), 1386-1395 (1993).
60. Akira Hasegawa and Yuji Kodama, "Amplification and reshaping of optical solitons in a glass fiber," Optics Letters, **7**(6), 285-287 (1982).
61. E.A. Kuznetsov, A.V. Mikhailov, I.A. Shimokhin, "Nonlinear interaction of solitons and radiation," Physica D **87**, 201-215 (1995).
62. Hermann A. Haus, Farzana I. Khatri, William S. Wong, Erich P. Ippen, and Kohichi R. Tamura, "Interaction of Soliton with Sinusoidal Wave Packet," Ieee Journal Of Quantum Electronics **32**, 917-924 (1996).
63. G. P. Agrawal, *Nonlinear Fiber Optics* (Academic Press, 2001).

1. Introduction

Airy pulses [1], whose electric field temporal profile is defined by an Airy function which is a one-sided, oscillating function having infinite energy, are a solution to the linear dispersion equation

$$i\frac{\partial A}{\partial z}=\frac{\beta_2}{2}\frac{\partial^2 A}{\partial T^2}, \tag{1}$$

and exhibit two interesting features: during propagation the waveform maintains its shape in the presence of dispersion and its wavefront accelerates in time (or travels along a ballistic trajectory) in a time frame moving at the group velocity. However, true Airy pulses are impractical as they contain an infinite amount of energy. By apodizing the Airy pulse, i.e. truncating the semi-infinite oscillations, in our case with a decaying exponential envelope, the waveform maintains its two unique properties over an extended propagation range despite its finite energy (Fig. 1(a)) [2]. Truncated Airy pulses occur naturally if a Gaussian pulse is propagated in a fiber at the zero dispersion point, under the influence of cubic dispersion.

In complete analogy to the Airy pulse solution to the dispersion equation (1), spatial Airy beams are a solution to the paraxial equation. Spatial Airy beams have been investigated extensively in the last few years, and found to be useful for various applications such as optical micromanipulation [3], optical switching [4], plasma channel generation [5], and laser filamentation [6]. More recently, temporal Airy pulses are being investigated, in the context of spatiotemporal light bullets in linear conditions [7] and in nonlinear conditions [8], and in the context of one dimensional Airy pulse propagation, under the influence of strong nonlinearity giving rise to supercontinuum and solitary wave generation [9].

In this study, we analyze temporal Airy pulse propagation in media exhibiting Kerr nonlinearity as occurring in single mode silica fibers, leading to the phenomena of self-phase modulation (SPM) and anomalous dispersion. The influence of the Kerr nonlinear effect on spatial Airy beams was investigated under relatively weak parameters and transient narrowing of the Airy main lobe—caused by SPM—was observed [10]; however, we are interested in operating under much higher intensities where the nonlinear effect results in soliton shedding from the Airy pulse and not just a small perturbation of the Airy beam. Although we analyze temporal Airy pulse propagation in fiber, our results are also valid for spatial Airy beams diffracting in Kerr media on account of the isomorphism between the dispersion equation (1) and the paraxial diffraction equation.

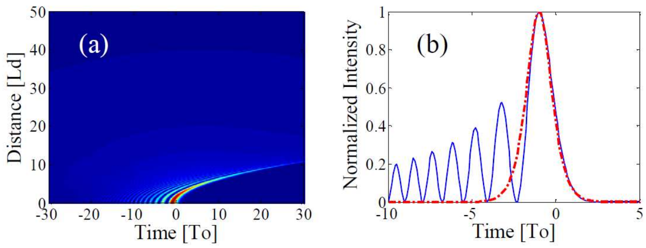

Fig. 1 – (a) Intensity distribution as a function of time and propagation distance for truncated Airy pulse in the linear regime (or low launch power). (b) Launched Airy pulse in time (blue solid curve), compared to a soliton pulse (red dashed curve).

The evolution of light pulses in single-mode dispersive-nonlinear medium is governed by the Nonlinear Schrödinger Equation (NLSE),

$$i\frac{\partial A}{\partial z} = \frac{\beta_2}{2}\frac{\partial^2 A}{\partial T^2} - \gamma |A|^2 A \tag{2}$$

where β_2 is the dispersion coefficient, γ is the nonlinear coefficient and A is the wave amplitude that depends on local time-T, and distance-z. Due to the addition of the nonlinear potential (or SPM term) in the NLSE, the Airy function is no longer a valid solution and we cannot predict analytically the Airy pulse evolution. The Soliton, on the other hand, is a well-known solution of the NLSE. For the canonical first order case, its profile is $\sqrt{P_0}\,\mathrm{Sech}(t/T_0)\cdot \mathrm{Exp}(iz\beta_2/T_0^{\,2})$, where P_0 is peak power and T_0 is duration and it is obtained only when there is equilibrium between the dispersion and the nonlinear effect, leading to the condition

$$P_0 \cdot T_0^{\,2} = \frac{|\beta_2|}{\gamma}. \tag{3}$$

The soliton then maintains its form and power level, provided no losses are present. Cases of perturbed soliton propagation (i.e. when there are small deviations from the condition set in Eq. 3) were extensively investigated [12-16], which help us interpret the emergent soliton behavior in our simulations.

In this paper, we propagate Airy pulses with different intensities and apodization values and investigate both the resulting 'emergent soliton' parameters, as well as the behavior of the residual Airy pulse. All our simulations are based on numerical solutions of the NLSE, using the split-step Fourier method (SSFM). This numerical method was chosen due to its efficiency in simulating one-dimensional pulse propagation [17].

Normalization terms

In our simulations we used the normalized NLSE form [17]

$$i\frac{\partial A}{\partial z}=\mathrm{sgn}(\beta_2)\frac{1}{2}\frac{\partial^2 A}{\partial T^2}-|A|^2 A, \tag{4}$$

where $|\beta_2|=\gamma=T_0=1$, and the launched Airy pulse profile is defined as:

$$A(T,z{=}0)=\sqrt{R\cdot K_p(a)}\cdot \mathrm{Ai}(T)\cdot \mathrm{Exp}(a\cdot T) \tag{5}$$

where 0‹a«1 is the truncation coefficient, and $K_p(a)$ is a truncation-dependent factor that sets the pulse peak intensity to 1 for any a value . This factor was numerically calculated and found to be in parabolic dependence with the truncation coefficient. T is the time variable in a frame of reference that moves with the wave group velocity, i.e. $T=t-z/v_g$, and R is a dimensionless parameter we vary for scaling the Airy power. At R=1 the Airy main lobe intensity profile looks quite similar to the fundamental soliton, as shown in Fig. 1(b).

We measure the propagation distance in L_d units, defined as $L_d=T_0^{\,2}/\beta_2$, which in our normalized coordinates equals 1.

2. Effects of launched Airy power

In order to investigate the influence of Airy launched power on its evolution, we varied the scaling parameter R in the range 0.1-2 and for every R value we propagated the pulse using the SSFM algorithm. Fig. 2 shows pulse evolution examples for select R values. At low launched power, the Airy pulse performs the acceleration in time and subsequently it succumbs to dispersion. However, when R is sufficiently large (above 0.9) a stationary soliton pulse is formed out of the centered energy about the Airy main lobe. The soliton exhibits periodic oscillations in the soliton amplitude and width as a function of propagation distance. In addition, we witness the resilience of the temporal Airy waveform to shedding of a fraction of the energy as a soliton; the wavefront continues to propagate along a parabolic trajectory. Similar resilience has been shown in main lobe masking for spatial Airy beams [11] and in supercontinuum generation for temporal Airy pulses propagation [9].

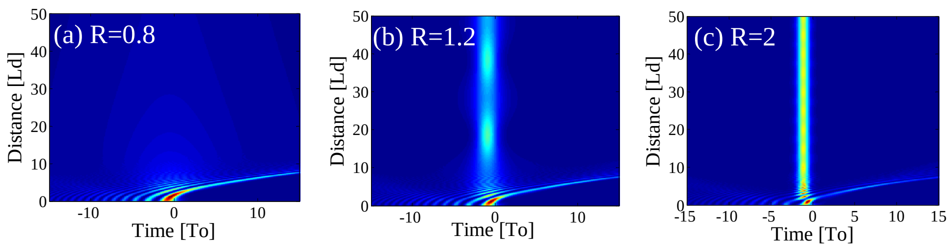

Fig. 2 – Intensity distributions as a function of time and propagation distance in the nonlinear propagation regime for: (a) R=0.8, (b) R=1.2, and (c) R=2.

The emergent soliton

Unsurprisingly, the shed pulse profile well conforms to a hyperbolic-secant function, or that of a soliton with background radiation. We fit a sech(·)+background radiation profile at every propagation distance and track the emergent soliton peak power, duration and time position along the propagation distance. We find that the power × duration^2 product oscillates about the equilibrium condition (=1) defined in Eq. (2). These oscillations about the stable soliton are known to arise as a result of interference between dispersive background radiation and the formed soliton [12, 13].

We examined the relations between the soliton oscillations and the launched Airy peak power. In Fig 3(a) the oscillations of soliton width are shown as a function of propagation distance for select R values. The pulse width narrows and the oscillations period decreases with higher launch power. The decreasing oscillation period with increasing launch power is depicted in Fig. 3(b). Similar behavior was reported in [13], where the amount of excess energy that was supplied to the launched soliton was expressed in the evolved soliton oscillations period. Another property of the oscillations is the modulation depth that sharply decreases with increased initial peak power (Fig. 3(c)). We can relate the low modulation depth to the greater stability of the formed soliton and conclude that high launched peak power is required for stable soliton formation.

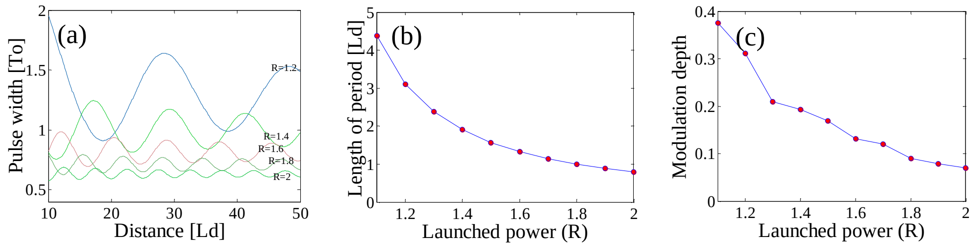

Fig. 3 – (a) Oscillations of soliton width for different launched peak power, (b) soliton oscillations length of period as a function of launched peak power, (c) soliton oscillations modulation depth as a function of launched peak power.

Additional soliton parameters as soliton peak time position and phase also oscillate in similar manner as the peak power and width. Fig. 4 (a, c) shows the evolution of time position and phase as a function of propagation distance (phase fluctuations are plotted after subtracting the soliton's accumulated linear phase term). These oscillations are the result of interaction with the background radiation as explained in [14] and demonstrated in [15] for the problem of background radiation that is formed by soliton amplification in optical communication.

From the results in Fig. 4(a) we see that the position of the emergent soliton is also dependent on launch power. We plot the mean time position of the emergent soliton in Fig. 4(b). More intense excitation results in the soliton appearing at an earlier time. This phenomena is explained by the fact that for low values of *R* a relatively long time is required for accumulation of enough energy by SPM for the soliton formation and shedding, and during this time the Airy pulse is accelerating and 'carries' the accumulating energy with it to later times. For larger *R* values there is enough energy in the Airy main lobe for soliton formation and shedding at an early point.

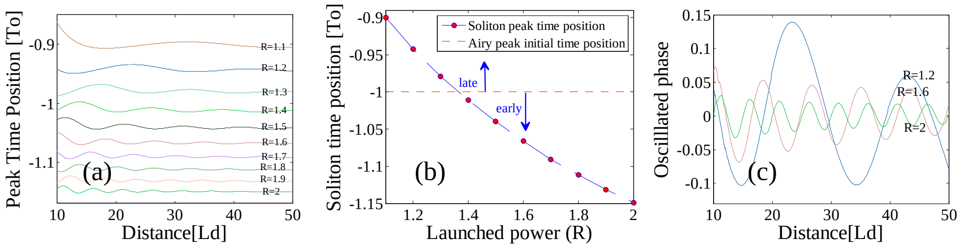

Fig 4 – (a) Soliton peak time position along propagation distance, (b) mean soliton peak time position as a function of launched power. Note that Airy peak time position at launch is at t=-1. (c) soliton peak phase oscillations along propagation distance for select launched powers.

The accelerating wavefront

As seen in Fig. 2, the Airy wavefront continues to exhibit the parabolic acceleration in time, even under the influence of Kerr effect and after shedding energy to the soliton. To study whether this acceleration continues with the properties of the linear propagation we compared the nonlinear propagations to linear, as the intensity is scaled with the *R* parameter. Note that the linear Airy pulse evolution is identical for every intensity value.

These linear propagation results are compared to the nonlinear ones by tracking the main lobe acceleration trajectory for each case and extracting information about its peak power and position. Furthermore, we calculate the accelerating energy distribution along propagation distance.

Fig. 5 shows the Airy main lobe parabolic trajectory and peak power as a function of propagation distance, under linear and nonlinear propagation, for three select launched power cases. We see that the wavefront continues to exhibit the parabolic trajectory in time (blue curves), which is almost identical in the linear and the nonlinear propagation cases, although the nonlinear peak slightly trails the linear peak, on account of a delay associated with the energy shedding to the soliton. The intensity evolution of the accelerating wavefront is shown in green. We can see that in the nonlinear propagation its peak power performs decaying oscillations, as opposed to the monotonic decay in the linear case. The oscillations of the peak power in the nonlinear case are known to be a result of the interplay between the SPM and the dispersion. Similar influence of SPM on the Airy accelerating main lobe was already observed in [10]. However, the peak power oscillations there exhibit faster decay due to a relatively large truncation coefficient, 0.1-0.3 vs. 0.0335 in the current simulations.

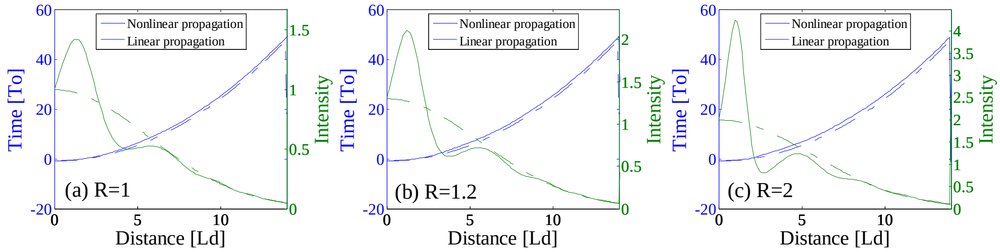

Fig. 5 – Airy accelerating tail trajectories in time-distance space(blue) and in intensity-distance space (green) for (a) R=1, (b) R=1.3 and (c) R=2.

Next, we investigate the energy distribution of the accelerating wavefront. It is important to note that the simulations preserve the launched pulse energy along the propagation distance, as well as preservation of 'center of gravity' (first order moment) position according to the finite pulse energy and the uniformity of the media [2]. The power spectrum of the Airy pulse is symmetric about the central frequency, and upon propagation in anomalous dispersive media the high frequencies components are delayed (low frequency components are advanced) with respect to central frequency group delay (in anomalous media), such that the pulse total energy is eventually divided to two equal fractions about T=0- half of the energy at each direction. In the presence of Kerr nonlinearity, considerable part of the pulse energy is shed to the soliton that propagates at the group velocity, and the remaining energy disperses in opposite directions with less than a half of the launched energy dispersing to each side (due to soliton shedding).

The energy that is carried in the accelerating wavefront (delayed components) was found by summing the energy over positive time at every distance sample. These calculations were performed with both the linear and nonlinear propagations.

Fig. 6(a) shows the delayed energy evolution of the accelerated Airy wavefront along the propagation distance for various Airy launched powers. The energy is normalized by the launched pulse energy, such that we can see the relative energy portion of the accelerating wavefront for linear and nonlinear cases. For all R values, the energy evolution of the linear propagations coincides to one curve that asymptotically approaches the value of half launched pulse energy, according to its linear nature. For the nonlinear propagations we clearly see that as R grows the fractional energy amount that is delayed is decreasing, where the oscillatory behavior is due to the soliton oscillations which take place in the boundary of the right half propagation plane. Those curves and those of Fig. 6(b), which chart the energy evolution of the formed soliton for different R values, show the fact that the formed soliton not only has more intensity when R is growing, but also carries a larger energy fraction from the whole pulse. This can also be seen in Fig. 6(c), where the mean soliton relative energy was calculated for every R value. From Figs. 6(b-c) we also see the energy preservation—the normalized delayed energy is missing energy that is about half of the shed soliton energy, where the other half originates from the faster propagating energy components. When R=2, for example, the soliton energy fraction is about 0.39 and the missing fractional energy amount from the delayed energy is about 0.19, half of 0.39.

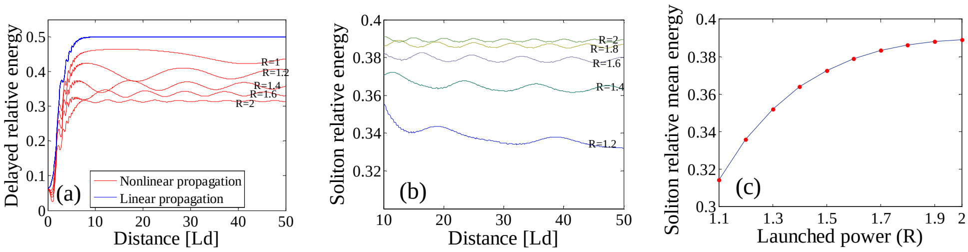

Fig. 6 – (a) Airy tail relative energy for the linear and the nonlinear cases, (b) soliton relative energy, (c) soliton relative energy as function of launched power.

3. Truncation coefficient effect

The ability of Airy pulses to exhibit their unique features is strongly related to the degree of truncation in the apodization function. As the truncation is stronger, the Airy pulse quickly loses the unique features of the Airy pulse and disperses. Here we wish to examine how the truncation degree influences the soliton shedding and pulse propagation under the Kerr effect.

We employ the same pulse profile defined in Eq. 4, fixing the intensity scaling parameter R to 1.5 while varying the truncation coefficient in the range 0.01-0.1, as shown in Fig. 7(a), and propagate the apodized Airy for every truncation value. Fig. 7(b-c) shows two examples of the Airy pulse evolution in time-distance space. We see that when the truncation is small the Airy original features as self-similarity and acceleration in time are more noticeable. The influence of the truncation degree on emergent soliton properties and on the accelerating wavefront was examined in the same manner as in the previous section.

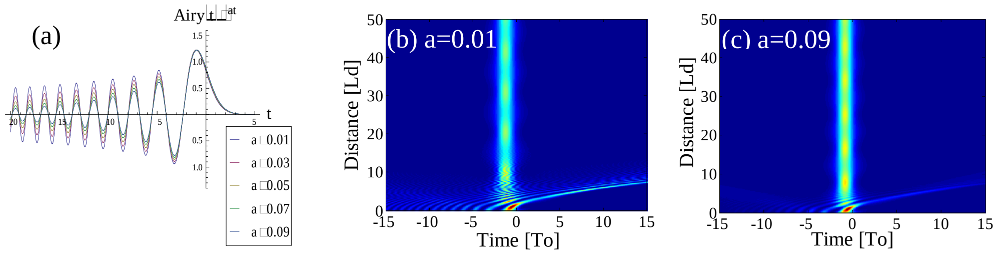

Fig. 7 – (a) Launched Airy amplitude for several truncation values, (b)-(c) Intensity distributions as a function of time and propagation distance for: (b) a=0.01, (c) a=0.09.

The emergent soliton

Larger truncation coefficient values make the exponential apodization of the Airy function stronger and the Airy tail is shortened; there is a negligible effect on the main Airy lobe, as shown in Fig. 7(a). Hence the emergent soliton , which forms from the main lobe, achieves stability faster (after a shorter propagation distance) in cases of larger truncation coefficients, as the newly formed soliton experiences less collisions with the accelerating Airy tail, as shown in the propagation images in Fig. 7. Therefore, the Sech(·) fit process was started from a different propagation distance for every truncation value.

From the soliton fit data we see that the emergent soliton parameters do not experience significant variations for different truncation values, as shown in the soliton parameters evolution curves in Fig 8(a-b). However, the soliton mean peak time position does shift considerably from the launched Airy peak position, and this shift increases for smaller truncation values (see Fig. 8(c)). This behavior is explained by the interaction between the formed soliton from the main lobe and the accelerating lobes of the Airy tail, which constitute collision perturbations to the soliton and cause temporal shift of the soliton in the direction opposed to the accelerating lobes [16]. This temporal shift to earlier times depends on the perturbation energy, which increases for small truncation coefficient values. It is important to note that even without perturbing lobes (i.e. while propagating Airy with strong truncation), the soliton is not necessarily formed at the launched Airy peak position because of the acceleration that the original pulse undergoes before the soliton is shed. Also, the launched Airy peak time position is not constant with different truncation coefficients (dashed red line in Fig 8(c)), as a result of a shift from the multiplication by the exponential apodization function.

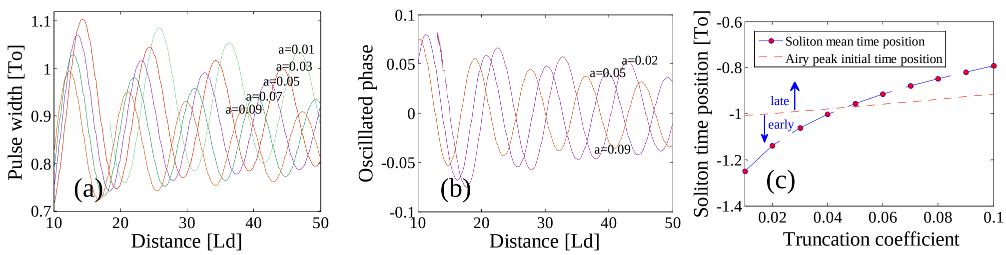

Fig. 8 – Effect of different launched truncation values on oscillations of (a) soliton width and (b) soliton peak phase, (c) soliton peak time position as function of truncation coefficient. Note that Airy peak time position at launch is truncation value dependent, as evidenced by the dashed red line.

The accelerating wavefront

The extent to which the truncated Airy maintains its form and continues to accelerate before dispersing strongly depends on the truncation coefficient. As in the previous section, we compared the linear and the nonlinear propagations in order to investigate the Airy's accelerating wavefront behavior for different truncation values. In the linear propagation regime, the truncation coefficient determines both the distance at which the accelerating wavefront is still distinguishable, and the total Airy energy according to $E_{Airy} = (8\pi a)^{-1/2}$ [2]. In our investigation range for truncation coefficient, the linear Airy varies widely.

After tracking the accelerating wavefront trajectory for every truncation value, we compare the main lobe trajectory and peak power under the linear and the nonlinear propagation regimes (Fig. 9). The main finding here is that the intensity of the accelerating main lobe in the nonlinear regime (green curves) first experiences SPM and focuses to the same peak power (with no dependence on truncation value). This peak is then shed to the soliton and the remaining accelerating wavefront immediately after the soliton shedding is at lower power compared to the linear propagation case. However, as a consequence of chromatic dispersion, the high frequency components travel slower and eventually the leading wavefront main lobe re-emerges and matches the main-lobe power of the linear propagation case (the Airy self-healing property). In spite of this wavefront matching between the linear and nonlinear propagations we see that in the nonlinear propagation the accelerating main lobe remains distinguishable for longer distances than in linear propagation for a given truncation value. This finding is related to the differences between the radiation energy distribution in the nonlinear and in the linear propagations. In the linear propagation (see example in Fig. 1(a)) the dispersed Airy intensity roughly converges to a Gaussian distribution in time with propagation distance that eventually (after a certain distance) engulfs the accelerating main lobe. In the nonlinear propagation the dispersive radiation intensity is no longer Gaussian distributed due to the soliton formation and the energy centering about it, making the accelerating peak visible for longer propagation distance.

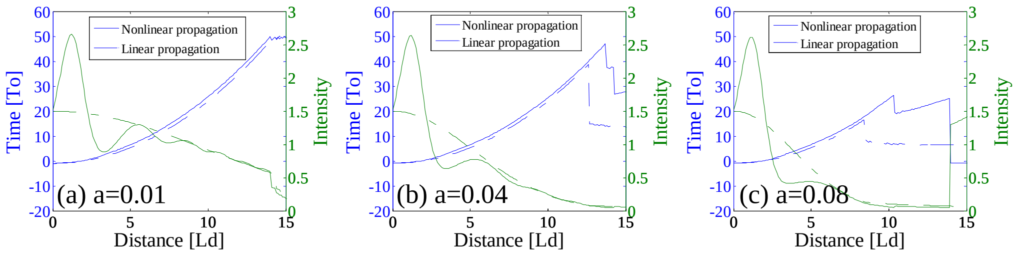

Fig. 9 – Airy accelerating wavefront trajectories in time-distance space (blue) and in intensity-distance space (green) for (a) a=0.01, (b)a=0.04 and (c)a=0.08.

As the emergent soliton has roughly the same energy for all truncation values, its relative energy fraction in the launched pulse energy is larger for increasing truncation values (Fig 10a), therefore the relative energy fraction in the accelerating Airy wavefront decreases (Fig. 10b). In the linear propagation regime the accelerating Airy energy always asymptotically approaches one half of the whole pulse energy, although its energy growth rate is truncation factor dependent. In the nonlinear case the delayed Airy energy fraction decreases from this value as the truncation is growing, as the nearly constant soliton energy is missing.

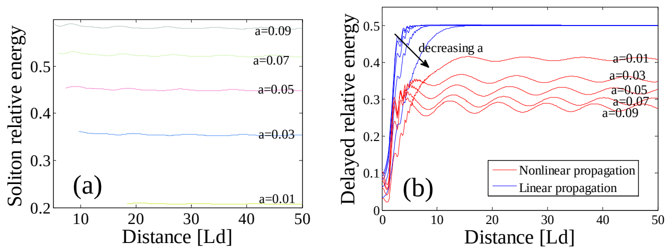

Figure 10 – Examples of energy evolution along propagation distance of (a) the relative energy of the emergent soliton (the soliton energy itself is hardly dependent on truncation coefficient) and (b) accelerating wavefront.

4. Soliton time position for power and truncation

In the previous sections we showed that: (1) the emergent soliton time position is at earlier times when the launched power increases (at fixed truncation) due to quick build-up of a soliton. At lower powers, self-focusing results in the eventual build-up of the soliton, but as the conditions materialize the main lobe is undergoing the ballistic trajectory leading to soliton shedding at a later time position. And (2) the emergent soliton time position is at earlier times when the truncation coefficient decreases (at fixed launched power) due to collision perturbations with the accelerating tail lobes. The time shift associated with collision perturbations depends on the energy; hence higher truncation coefficients result in lower Airy tail energies and reduced soliton time shifts. These two effects are graphically depicted in Fig. 11(a).

To verify that these two effects independently and consistently occur, we varied both the Airy launched power and the truncation coefficient over our investigation range (Fig, 11(b)). Indeed we see this trend continuing; the emergent soliton mean time position shifts to earlier (later) times for smaller (larger) truncation coefficients and for higher (lower) launched power levels. These results reinforce our finding that soliton is shed at an earlier time when the launched power is higher, and that collisions with the accelerating Airy tail lobes shift the position in the direction counter to the acceleration, i.e. towards earlier times.

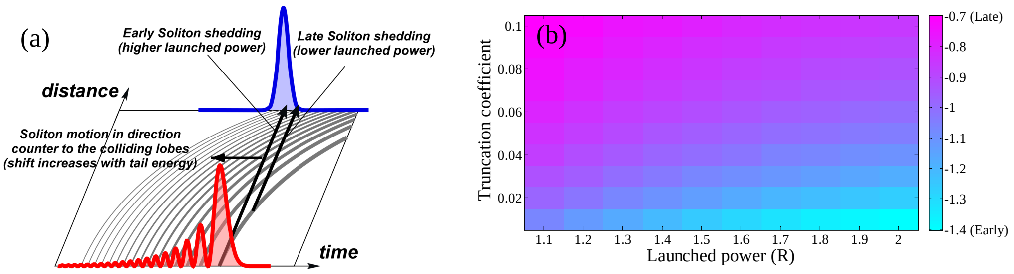

Figure 11 – (a) Schematic illustration of the sources of temporal shift of the emergent Soliton. (b) Distribution of Soliton mean time position as a function of truncation coefficient and launched power in our investigation range.

5. Summary

In this paper we investigated the propagation of a truncated temporal Airy pulse in nonlinear Kerr media. The phenomena of soliton shedding from the original Airy pulse under sufficiently strong excitation was already identified [8,9], but in this work we investigated in detail the properties of the soliton and the remaining Airy radiation. We characterized the emergent soliton parameters under different truncation and power conditions and identified the mechanisms at play, in accordance to processes known from literature. The soliton parameters perform oscillations due to the presence of background radiation from the dispersed Airy pulse. The temporal position of the emergent soliton depends both on the Airy launched power and truncation coefficient, due to the location of the shedding event and the interaction with the accelerating Airy tail. We also observed the SPM influence on the accelerating Airy main lobe, and we found that the SPM has large effect on the accelerating main lobe visibility in comparison the linear truncated Airy propagation. Finally, we found that the energy distribution of the Airy pulse along the propagation depends on the launched power and the truncation degree.

In this work we studied the soliton shedding phenomena for relatively intense launched Airy pulses. This research avenue can continue to even higher launched pulse powers, however eventually the well-understood phenomena explored here starts to break down. Fig. 12 shows the time-space evolution when launching the Airy pulse with a power factor of four (R=4). We see that for such intense excitation three solitons are shed, the main soliton in a consistent manner to that described here, and two additional weaker soliton s at both higher and lower center frequencies. This result was still obtained with the standard nonlinear Schrodinger equation (Eq. 4). However, for proper simulation of intense Airy pulse excitation, one should also add additional terms to account for higher-order nonlinear effects such as Raman scattering and self-stepping.

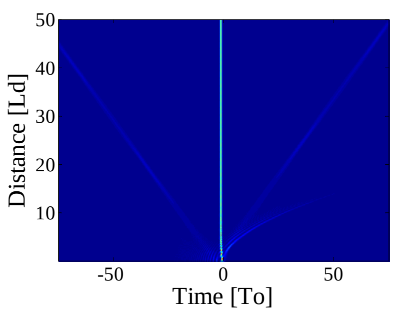

Figure 12 – Intensity distributions as a function of time and propagation distance for R=4, showing multiple soliton shedding at high launched peak powers.